REWRITING THE TROPICAL RECORD BOOKS

The Extraordinary Intensification of Hurricane Patricia (2015)

Robert F. Rogers, Sim Aberson, Michael M. Bell, Daniel J. Cecil, James D. Doyle, Todd B. Kimberlain, Josh Morgerman, Lynn K. Shay, and Christopher Velden

East Pacific Hurricane Patricia (2015) broke several records, including intensification rate and peak intensity. An impressive array of observations was collected in this storm for much of its life cycle.

In late October 2015, a remarkable meteorological event unfolded off the west coast of Mexico. At first, the event seemed like a typical east Pacific tropical cyclone (TC), with operational forecasts of it becoming a minimal hurricane at best. What actually transpired would rewrite the record books for TCs. Hurricane Patricia became a historic storm, breaking several records, including those related to rate of intensity change and peak intensity [Table 1,[1] derived from Kimberlain et al. (2015)]. These records, some of which have been recognized by the World Meteorological Organization (WMO), are valid for either the entire globe or the Atlantic and east Pacific basins specifically. Based primarily on the analyses of the National Hurricane Center (NHC), the WMO's Archive of Weather and Climate Extremes, a compendium of internationally accepted extremes (https://wmo.asu.edu/), now lists Hurricane Patricia as "most intense (by central pressure) tropical cyclone (Western Hemisphere)" with an estimated mean sea level pressure of 872 hPa as occurring on 23 October 2015. This value is second only to the 870-hPa value for Typhoon Tip on 12 October 1979. Additionally, the value of 185 kt (~95 m s^{-1}) as an estimate of peak maximum sustained near-surface winds is accepted as "most intense (by maximum sustained surface winds) tropical cyclone (Western Hemisphere)" and ties the record for the globe with Typhoon Nancy's (1961) estimated winds.

[1] An important context is that the historical record is incomplete in terms of how other TCs might compare to Patricia. Most of the intense hurricanes in the Atlantic have been sampled by reconnaissance or research aircraft, and the observational capabilities of those aircraft have increased over the years. Few hurricanes in the eastern Pacific have been sampled by such aircraft. Even fewer in other basins have had direct observations suitable for addressing the metrics in Table 1, since western North Pacific reconnaissance ceased in 1987. Even with the benefit of aircraft observations, there remain questions for Patricia and many other hurricanes about how the intensity evolved before and after aircraft fixes of the center. Table 1 lists records that were set by Hurricane Patricia, relative to this inherently limited historical record. Some of the records are based on the "best tracks," which compile official best estimates of intensity for every TC. There is necessarily large uncertainty, but that is the state of such records.

The primary forecast challenge with Patricia was that it intensified at a rate far exceeding the traditional definition of rapid intensification [defined as an increase in the 1-min average wind speed at 10-m altitude in excess of 35 kt (~18 m s^{-1}) in 24 h in the east Pacific; Kaplan et al. (2010)] and also weakened at an unprecedented rate. Such extreme rates of intensity change present significant challenges to both operational forecasting agencies and forecast models. Dynamical and statistical models, and the consensus techniques incorporating them, provide guidance for operational forecasting agencies, but these often are limited, especially in a case like Patricia. Consider the intensity forecasts from a selection of operational models at 0600 UTC 21 October (Fig. 1), when Patricia had just been designated a 35-kt (~18 m s^{-1}) tropical storm. During the next 48 h, none of the forecast guidance, including the most sophisticated, highest-resolution, fully coupled operational models and the best-performing statistical/dynamical models, forecast Patricia to have a maximum sustained wind speed above 100 kt (~51 m s^{-1}). During this time, however, Patricia intensified to 185 kt (~95 m s^{-1}), a strong category 5 hurricane on the Saffir–Simpson hurricane wind scale and the strongest ever measured. The observed intensification rate was more than double what any of the forecast guidance predicted. Even after Patricia had reached 55 kt (~28 m s^{-1}) at 0000 UTC 22 October 2015, the dynamical models had intensification rates less than half what actually occurred (not shown). The subsequent weakening rates were equally dramatic. While forecasting these rapid intensity changes is beyond our current capabilities, attempting to understand the reasons behind them can help to improve future predictions of such extreme events.

Patricia was sampled by a variety of airborne in situ and remote sensing instruments during much of its life cycle. The aircraft that sampled Patricia were flown as part of the Office of Naval Research (ONR) Tropical Cyclone Intensity experiment (TCI; Doyle et al. 2017), the National Oceanic and Atmospheric Administration (NOAA) Intensity Forecasting Experiment (IFEX; Rogers et al. 2006, 2013a), and operational aircraft reconnaissance. The measurements included high-resolution, full-tropospheric dropsonde kinematic and thermodynamic profiles (Hock and Franklin 1999), wide-swath measurements of surface wind speed, and airborne conventional and Doppler radar measurements of kinematic and precipitation structure. Though flight-level and airborne Doppler measurements have been collected in many Atlantic and some east Pacific TCs, what makes this dataset exceptional are the high-density, high-altitude dropsonde and wide-swath surface wind speed measurements. These aircraft observations, combined with various satellite-derived observations and detailed in situ measurements of surface pressure collected from mobile platforms very near the landfall point, allow for a detailed analysis of the kinematic and thermodynamic structure during Patricia's life cycle.

This paper documents the structure and evolution of Hurricane Patricia using the aforementioned observations as it explosively intensified from a tropical storm to a category 5 hurricane, subsequently rapidly weakened, and made landfall on the Mexican coast. Some of the thermodynamic and kinematic structures observed in Patricia are compared to those from previous storms, including the Hawkins and Imbembo (1976) warm-core composite. Such observations provide an opportunity to explore the physical processes underlying the extraordinary rapid intensity changes associated with Patricia and evaluate their representation in numerical models.

SUMMARY OF AIRCRAFT MISSIONS.

The TCI field campaign used the National Aeronautics and Space Administration (NASA) WB-57 high-altitude jet that flies up to ~20-km altitude, above the TC outflow layer, with a typical flight duration of 6 h. The payload included the High-Definition Sounding System (HDSS; Black et al. 2017) and Hurricane Imaging Radiometer (HIRAD; Cecil and Biswas 2017). The HDSS is an automated

AFFILIATIONS: Rogers and Aberson—NOAA/Atlantic Oceanographic and Meteorological Laboratory/Hurricane Research Division, Miami, Florida; Bell—Colorado State University, Fort Collins, Colorado; Cecil—NASA Marshall Space Flight Center, Huntsville, Alabama; Doyle—Naval Research Laboratory, Monterey, California; Kimberlain—NOAA/NWS/National Hurricane Center, Miami, Florida; Morgerman—iCyclone, West Hollywood, California; Shay—Rosenstiel School of Marine and Atmospheric Sciences, University of Miami, Miami, Florida; Velden—Cooperative Institute for Meteorological Satellite Studies, University of Wisconsin–Madison, Madison, Wisconsin
CORRESPONDING AUTHOR: Robert Rogers, robert.rogers@noaa.gov

The abstract for this article can be found in this issue, following the table of contents.
DOI:10.1175/BAMS-D-16-0039.1

In final form 6 February 2017

Table 1. List of records broken/tied by Hurricane Patricia (2015), including sources (footnotes).		
Record	**Value**	**Valid region**
Highest 10-s peak sustained surface winds measured by aircraft (SFMR)[a]	94 m s^{-1} (182 kt)	Global
Highest 10-s peak flight-level winds measured by aircraft (700-hPa level)[a]	99 m s^{-1} (192 kt) (tied with Super Typhoon Megi 2010)	Global
Lowest minimum pressure estimated by aircraft[b]	879 hPa	ATL, EPAC
Warmest 700-hPa flight-level temperature measured by aircraft[a]	32.2°C	ATL, EPAC
Highest maximum 10-m sustained wind speed (Vmax) (best track)[c]	95 m s^{-1} (185 kt)	Global
Lowest minimum pressure (best track)[c]	872 hPa	ATL, EPAC
Most rapid intensification rate (best track)[a,c,d]	24 h: 97 hPa; 54 m s^{-1} (105 kt) [97 hPa (24 h)$^{-1}$ ties Wilma (2005)]	Global
Most rapid overwater weakening rate[a]	54 hPa, 26 m s^{-1} (50 kt) in 5 h	ATL, EPAC
Strongest updraft measured by dropsonde[e]	27.4 m s^{-1} (~53 kt)	Global
Highest advanced Dvorak technique T number[f]	T8.4 (94 m s^{-1}; 182 kt)	Global

[a] Kimberlain et al. (2015).

[b] WMO Weather and Climate Extremes Archive (https://wmo.asu.edu).

[c] International Best Track Archive for Climate Stewardship (IBTrACS; Knapp et al. 2010).

[d] Hoarau (2000) argues that Super Typhoon Forrest (1983) deepened by 101 hPa in 24 h based on extrapolations from the 700-hPa aircraft flight level, and the China Meteorological Administration best track lists 104-hPa deepening in 24 h, but other best tracks including Regional Specialized Meteorological Center (RSMC) Tokyo list 90 hPa (24 h)$^{-1}$ as Forrest's maximum deepening.

[e] Stern et al. (2016).

[f] Velden et al. (2017).

system deploying the expendable digital dropsonde (XDD) designed to launch dropsondes at high temporal rates (spatial intervals as small as ~4 km) to measure wind, pressure, temperature, and humidity profiles and skin sea surface temperature (SST). HIRAD is a C-band synthetic thinned-array passive microwave radiometer used to retrieve surface wind speed and rain rate across a wide swath (~50-km swath from an aircraft flying at 20-km altitude). Its retrieval concept is similar to the operational Stepped Frequency Microwave Radiometer (SFMR; Klotz and Uhlhorn 2014), with wind speed being related to the near blackbody emissions from foam on the roughened ocean surface.

For IFEX, the NOAA WP-3D aircraft flew at an altitude of ~2.5–3.5 km for a duration of ~8 h. The primary instruments on the WP-3D include the airborne tail

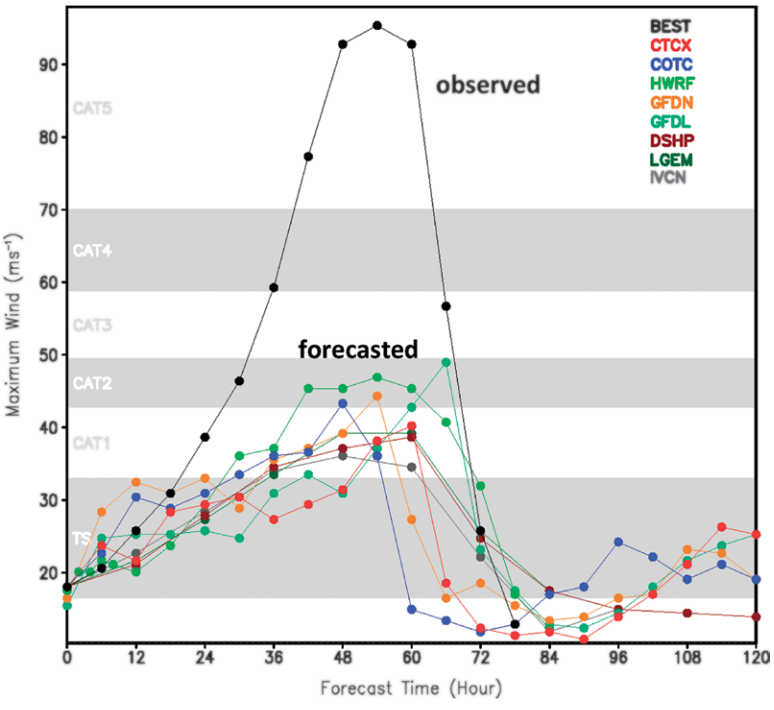

Fig. 1. Intensity forecasts from a suite of dynamical and statistical–dynamical models for Patricia valid 0600 UTC 21 Oct. Best track intensity trace indicated by black line [courtesy of Hao Jin and Naval Research Laboratory (NRL)].

Doppler radar, an X-band radar that provides reflectivity and radial (relative to the radar location) wind components in the presence of scatterers, a C-band radar mounted on the lower fuselage that provides reflectivity, dropsondes, flight-level instruments that measure standard atmospheric parameters, and the SFMR. Though no airborne expendable bathythermographs were deployed, ocean conditions were measured by several Argo profiling floats (e.g., Roemmich et al. 2009), and these measurements were consistent with those from satellites before the passage of Patricia. The U.S. Air Force C-130 has flight-level, SFMR, and dropsonde capabilities similar to those of the WP-3D.

Both aircraft operated out of Harlingen, Texas, overflying Mexico to reach Patricia. Figure 2 shows the flight tracks of both aircraft, overlaid on Geostationary Operational Environmental Satellite East (GOES-East) visible imagery at the approximate center time of each set of missions. On 20 October (Fig. 2a), only the

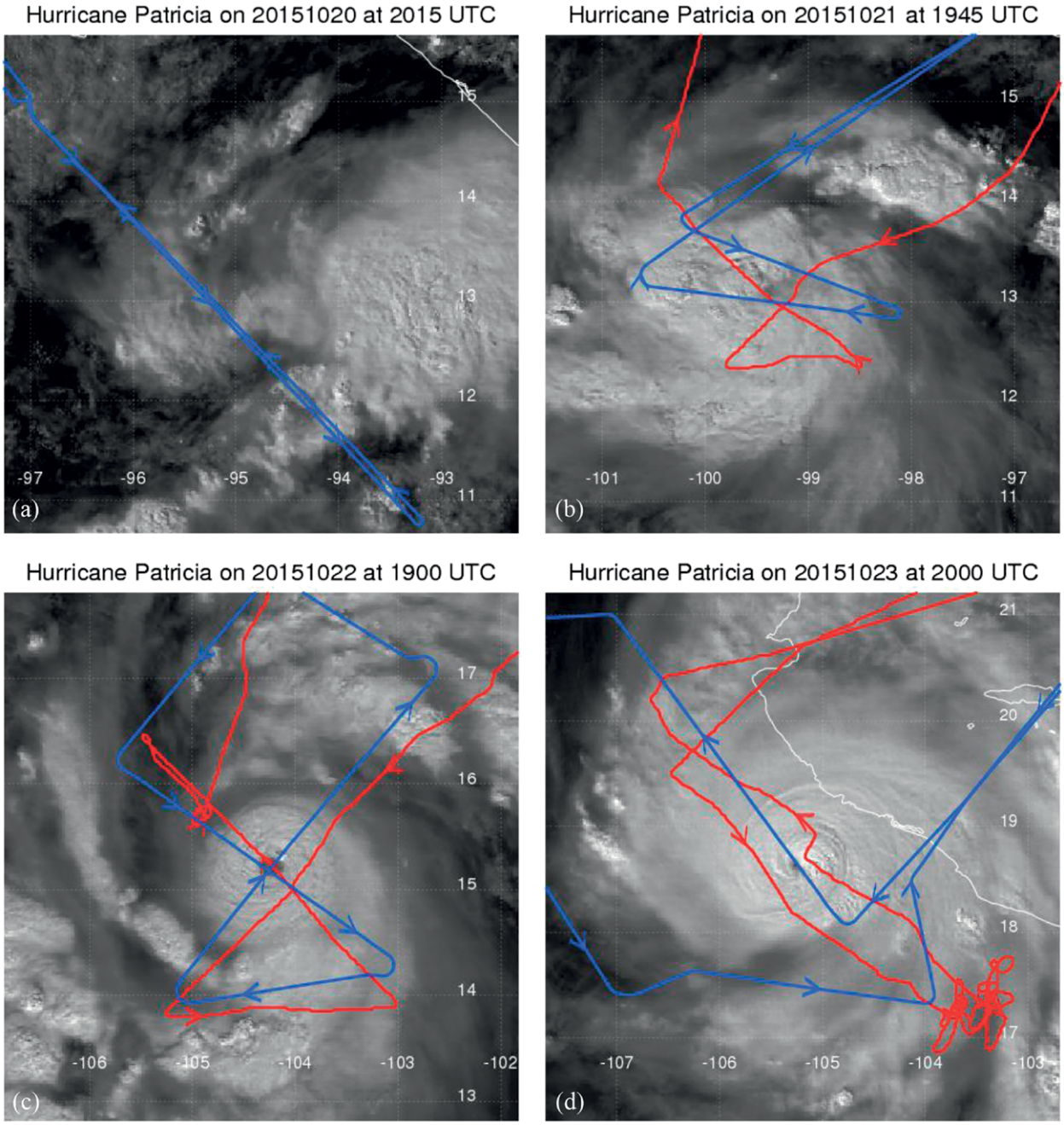

Fig. 2. Flight tracks and visible satellite imagery corresponding to the approximate midpoint of the aircraft missions. Blue is WB-57; red is WP-3D.

WB-57 sampled Patricia, flying a leg oriented northwest (NW)–southeast (SE) and back again. Both aircraft flew in Patricia on 21 October as it was getting organized (Fig. 2b). The WB-57 flew another NW–SE-oriented leg, with a return leg oriented east (E)–west (W), while the WP-3D flew a "figure 4" pattern, with the first center pass oriented northeast (NE)–southwest (SW) and the second oriented SE–NW. On 22 October, when Patricia was rapidly intensifying, both aircraft executed figure-4 patterns (Fig. 2c), with both having center passes oriented NE–SW and SE–NW. In addition to the WP-3D and WB-57 missions, the Air Force C-130 completed an NHC-tasked reconnaissance mission on 22 October, taking off from and returning to its base at Keesler Air Force Base, Mississippi. The C-130 completed a repeated figure-4 pattern (not shown) between WP-3D missions, arriving during the night of 22 October and leaving in the early morning hours of 23 October. Later on 23 October (Fig. 2d), when Patricia was near its peak intensity and beginning to rapidly weaken, the WP-3D encountered significant turbulence on its first pass through the center from the NW to the SE, requiring the aircraft to loiter on the SE side of Patricia while potential damage to computer equipment was assessed. The WB-57 completed a single center pass oriented SE–NW, followed by a sampling of the near environment on the west and south sides of Patricia. The WP-3D then completed its final center pass from the SE to the NW.

ENVIRONMENTAL CONDITIONS AND STORM EVOLUTION. Patricia's track and intensity from the official NHC best track are shown in Fig. 3. Patricia's development into a TC involved the interaction of multiple weather systems during

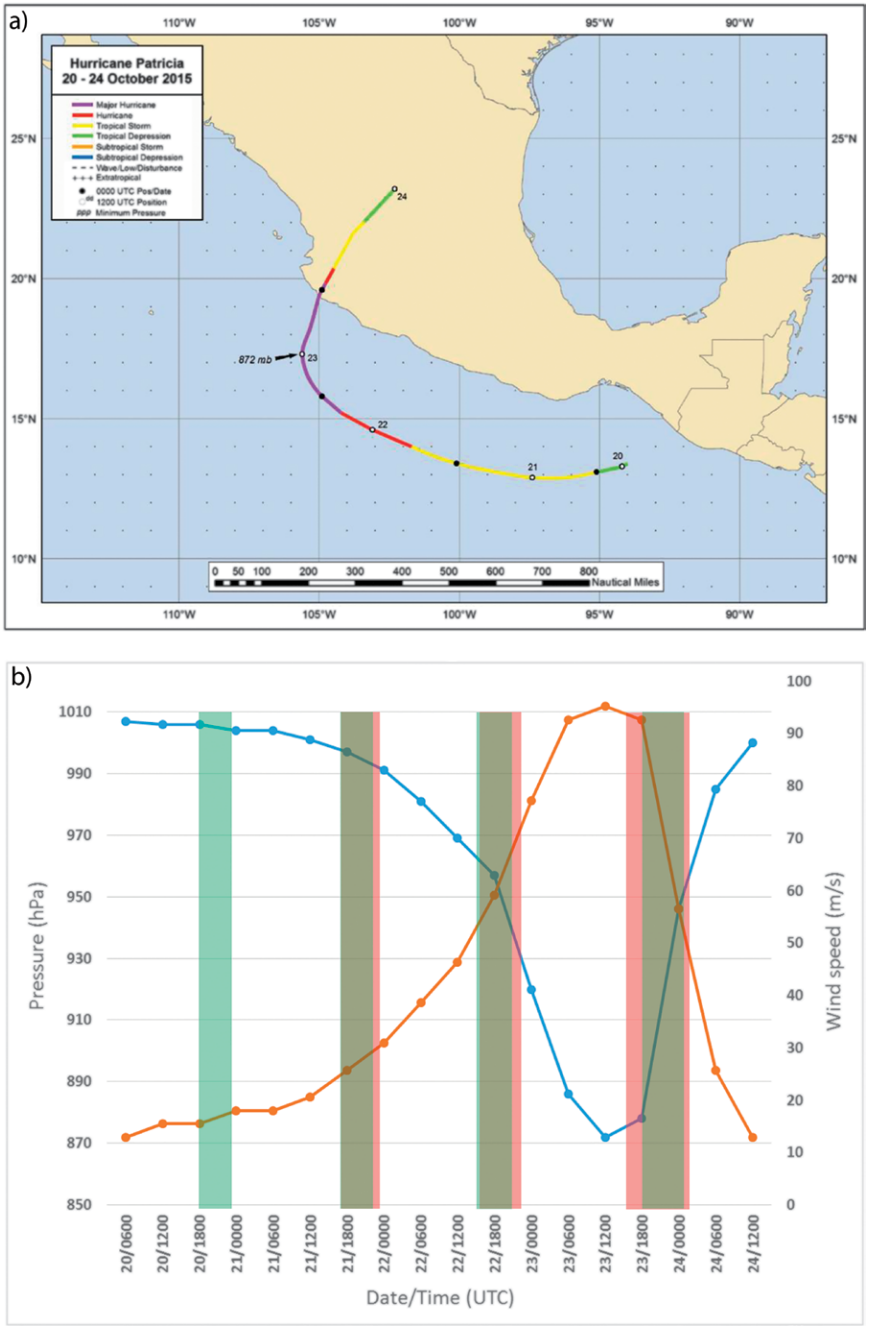

Fig. 3. (a) Final best track plot for Patricia [courtesy NHC and Kimberlain et al. (2015)]; (b) final best track intensity trace for Patricia. Blue line denotes minimum sea level pressure (hPa); orange line denotes peak 10-m winds (m s^{-1}). Green boxes in (b) denotes approximate takeoff and landing times for the WB-57; red boxes denote approximate takeoff and landing times for the WP-3D. Note: actual on-station times will be less than this, given the relatively long ferry time.

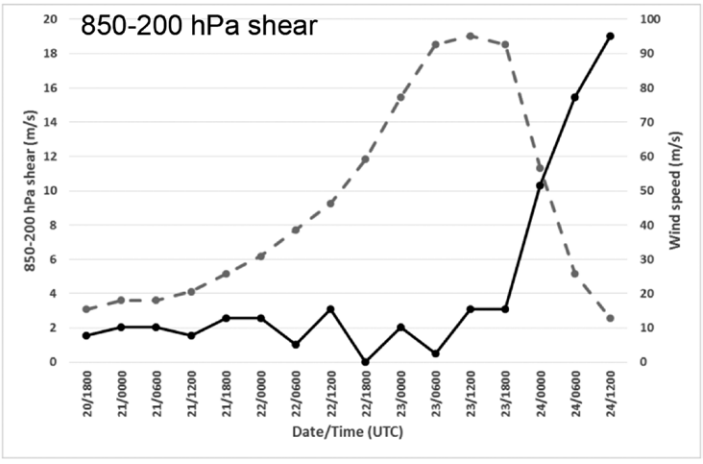

(a)

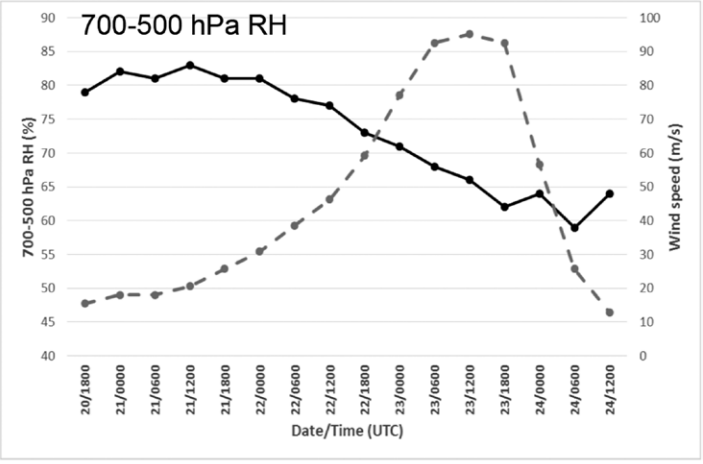

(b)

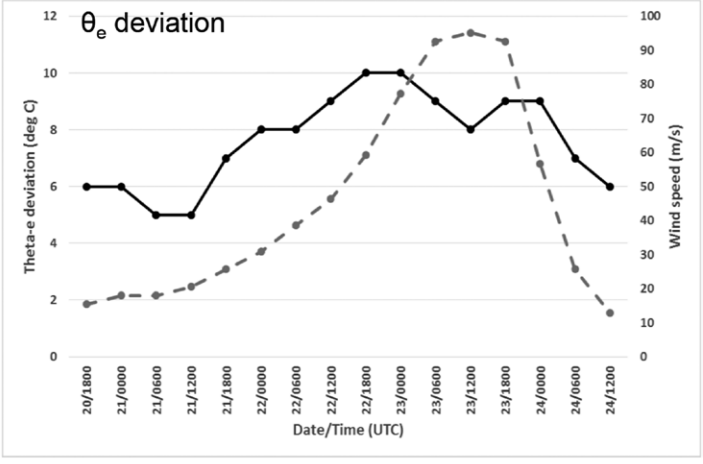

(c)

Fig. 4. Time series of large-scale environmental parameters from SHIPS diagnostics (DeMaria et al. 2005) using Global Forecast System (GFS) analyses. (a) 850–200-hPa vertical shear magnitude (m s^{-1}); (b) 700–500-hPa relative humidity (%); (c) surface–200-hPa θ_e deviation of lifted parcel. (a) Averaged within 0–500 km of center; (b),(c) averaged within 200–800 km of center. The dashed line indicates best track intensity (m s^{-1}).

several days (Kimberlain et al. 2015). A series of Gulf of Tehuantepec gap wind events interacted with an existing tropical wave from 16 to 19 October. These events injected cyclonic vorticity into the disturbance (Levine 2012; Holbach and Bourassa 2014; Hurd 1929) and may have enhanced its early development. Deep convection associated with a large cyclonic gyre increased substantially during this time, possibly owing to favorable large-scale conditions associated with the passage of the rising branch of a strong Madden–Julian oscillation moving across the eastern Pacific (not shown). An Advanced Scatterometer (ASCAT; Figa-Saldaña et al. 2002) pass around 0400 UTC 20 October (not shown) suggested that a small, well-defined circulation had developed underneath the convection within the large cyclonic envelope that was elongated from north to south, and the disturbance was declared a tropical depression at 0600 UTC 20 October about 180 n mi (~333 km) south-southeast of Salina Cruz, Mexico.

The depression was located to the south of a midlevel ridge centered over the Gulf of Mexico that extended west-southwestward into the eastern Pacific (not shown). The depression drifted west-southwestward while gradually strengthening, and it became Tropical Storm Patricia 18 h after genesis. By early 21 October, environmental conditions, as diagnosed by the Statistical Hurricane Intensity Prediction Scheme (SHIPS; DeMaria et al. 2005), showed that Patricia was encountering quite low (~2 m s^{-1}) deep-layer (i.e., 850–200 hPa) shear (Fig. 4). However, the storm was in a relatively stable environment over SST that was at least 2°C lower than the surrounding region (Fig. 5)—a result of the strong gap winds. This less favorable thermodynamic environment limited development, with deep convection temporarily diminishing and cloud-top temperature increasing late 20 October and early 21 October. Once Patricia moved outside this region, a rapid increase in deep convection occurred over the low-level center, and a small central

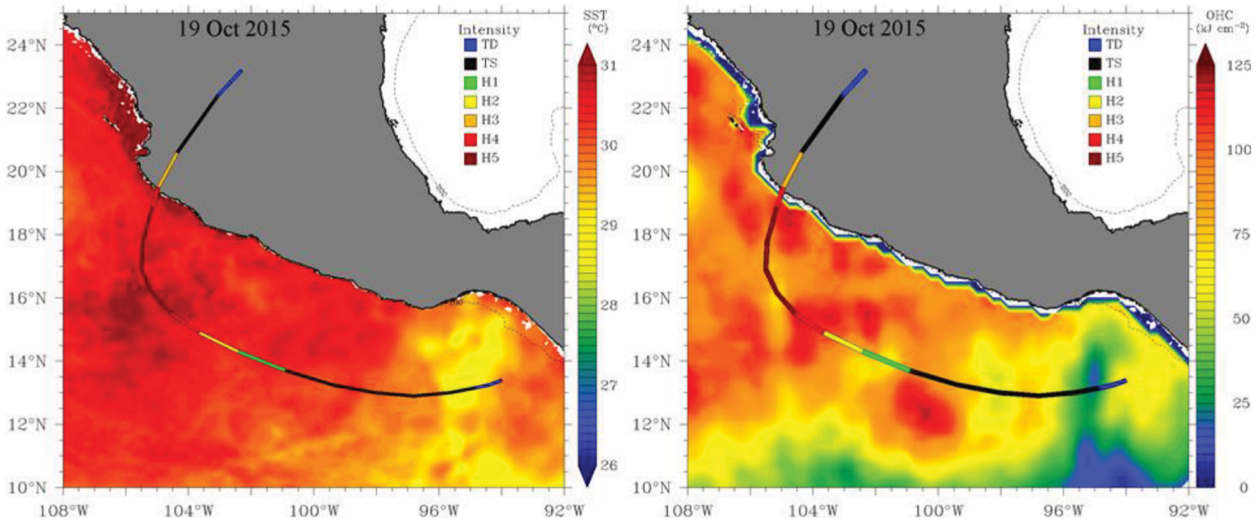

Fig. 5. (left) SSTs (°C) and (right) OHC (kJ cm^{-2}) on 19 Oct 2015 in the eastern Pacific Ocean prior to the passage of Hurricane Patricia. The track is colored based on intensity as per the inset in both panels. The OHC is based on SPORTS climatology where the sea surface height anomaly (SSHA) fields were from *Jason-2*, *Altika* (*SARAL*), and *Cryosat-2* missions.

dense overcast (CDO) began to form. Large-scale upper-level outflow conditions were favorable, with dual outflow channels evident on the west to north, and on the southeast through southwest sides of the storm, as depicted by satellite-derived wind vectors (Fig. 6). The atmospheric environment at this time was quite favorable for rapid intensification, with very light vertical wind shear, and high moisture and instability (cf. Fig. 4).

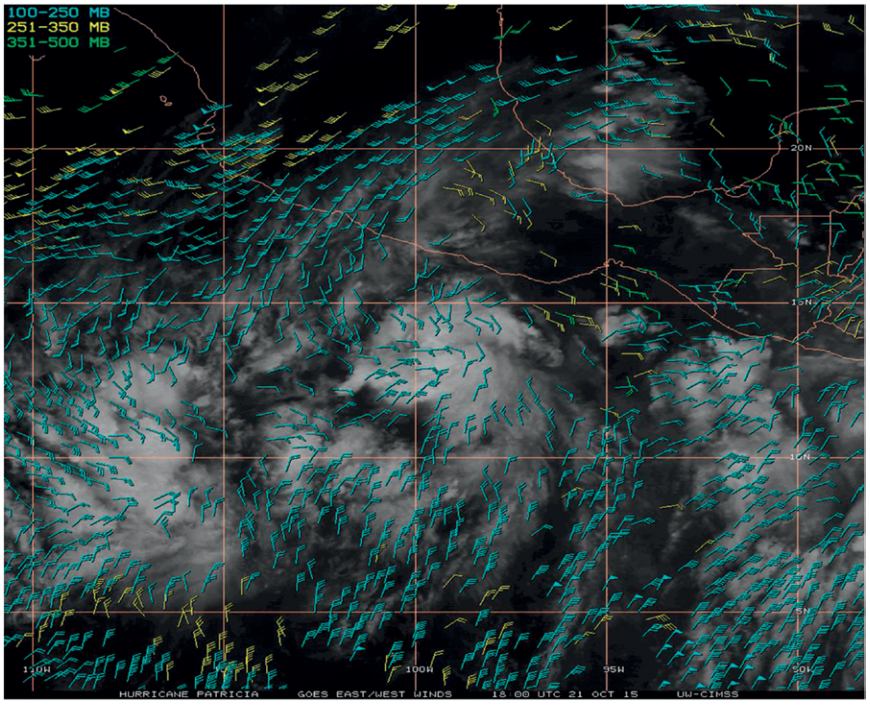

Fig. 6. Upper-level satellite-derived winds (m s^{-1}) on GOES IR imagery centered on Patricia at 1800 UTC 21 Oct 2015. Flag denotes wind speeds ~25 m s^{-1}; full barb denotes wind speeds ~5 m s^{-1}; half barb denotes wind speeds ~2.5 m s^{-1}. Blue barbs denote winds in the 100–250-hPa layer; yellow barbs are the 251–350-hPa layer; green barbs are 351–500-hPa layer.

The oceanic conditions were also quite favorable for significant intensification, as Patricia was located over water with SST values obtained from NOAA geostationary satellites (Maturi et al. 2008) near 31°C (Fig. 5). The corresponding ocean heat content (OHC) approached 90 kJ cm^{-2} in the observed warm pools in the region where Patricia explosively deepened (McCaskill et al. 2016). This OHC level is approximately a factor of 2 larger than the normal conditions in the eastern Pacific Ocean (Shay and Brewster 2010). Note the 2015 calendar year was an exceptionally strong El Niño year as shown by the Niño-3.4 index where values ranged from 2.1° to 2.3°C over the last few months of 2015. As shown in Fig. 7, both the 26°C isotherm depth and the OHC

values were significantly above the normal value by almost a factor of 2 in the August to November time frame. The 26°C isotherm depth increased to about 60 to 65 m while the associated OHC values exceeded 80 kJ cm^{-2} along Patricia's track. The corresponding increase in the sea surface height anomaly was approximately 12 cm above the normal (not shown). Compared to the other El Niño years, the 2015 signals were also significantly higher than previous El Niño years. These abnormally high OHC levels may have impacted Patricia's intensification through enhanced and sustained fluxes of heat and moisture as observed in other hurricanes moving over deeper and warmer thermal structure such as Hurricane Earl (Jaimes et al. 2015). Given the favorable atmospheric and oceanic environment, Patricia strengthened into a hurricane shortly after 0000 UTC 22 October while centered about 200 n mi (~370 km) south of Acapulco, Mexico.

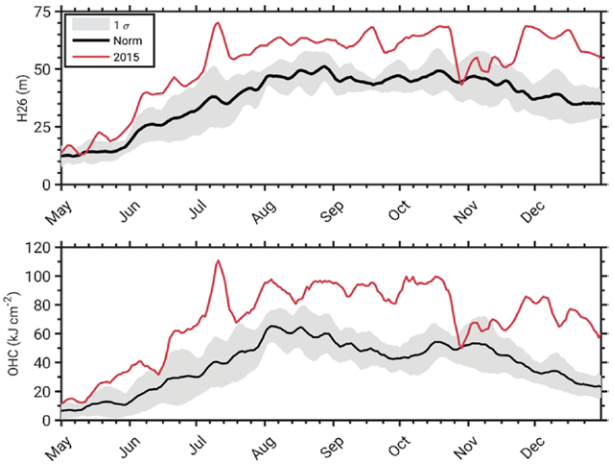

Fig. 7. (top) Satellite-derived estimates of the 26°C isotherm depth (m) and (bottom) the corresponding OHC (kJ cm^{-2}) from a 1° × 1° box centered along Patricia's track (17°–18°N, 104°–105°W) from May through Dec 2015 (red curves) compared to the normal time series representing the average of non-ENSO years of 2001, 2003, 2004, 2005, 2012, 2013, and 2014 with the one standard deviation depicted in gray based on the 3.4 oceanic Niño index (ONI) (www.cpc.ncep.noaa.gov/products/analysis_monitoring/ensostuff/ensoyears.shtml).

During the next 24 h, Patricia's satellite presentation changed dramatically, as a large convective band with cloud-top temperatures of –80° to –90°C evolved into an almost perfectly symmetric CDO around a 10 n mi (~18 km)-wide eye, and a favorable upper-level environment continued with well-established dual outflow channels (Fig. 8). The NOAA WP-3D aircraft arrived around 1800 UTC 22 October and indicated that Patricia had already reached major-hurricane intensity, with an estimated surface wind speed of 115 kt (~59 m s^{-1}) and a minimum pressure of 957 hPa. The exceptionally rapid intensification phase continued into the night while Patricia turned northwestward and its forward speed decreased, and satellite imagery indicated that a solid ring of cloud-top temperatures colder than –90°C surrounding a 7 n mi (~13 km)-wide eye had formed by 0300 UTC 23 October (not shown). By the time an Air Force Hurricane Hunter aircraft reached the TC around 0600 UTC, Patricia had intensified into an extremely powerful hurricane with a maximum sustained wind speed of 180 kt (~93 m s^{-1}) and a minimum central pressure of around 879 hPa. The highest flight-level wind obtained during Patricia, 192 kt (~99 m s^{-1}), was measured in the northeastern eyewall by the C-130, along with a maximum

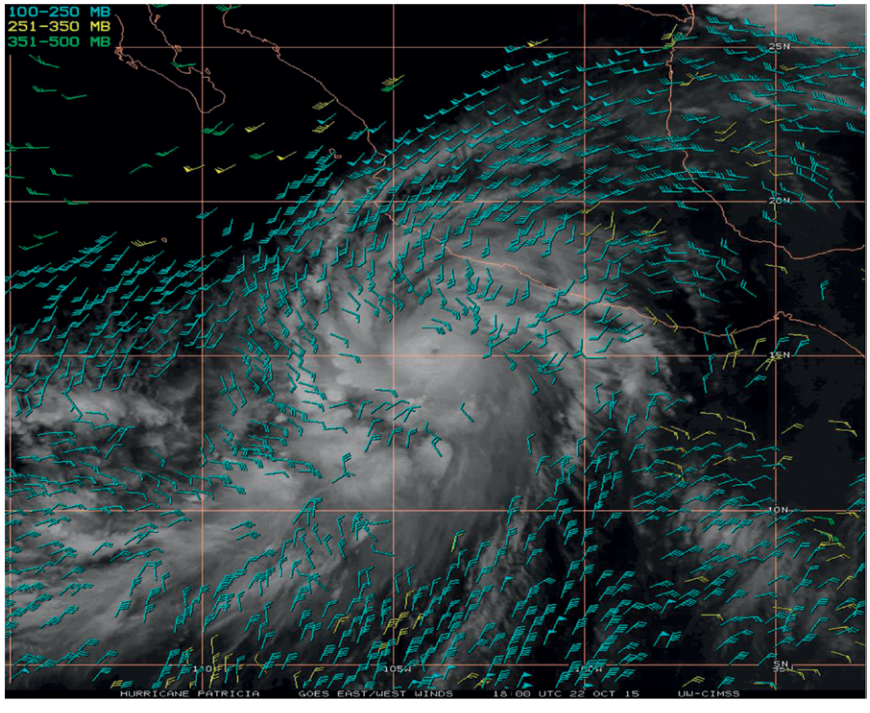

Fig. 8. As in Fig. 6, but for 1800 UTC 22 Oct.

observed surface wind speed from the SFMR of 182 kt (~94 m s^{-1}).

The satellite presentation continued to improve during the next several hours, and Patricia is estimated by NHC postanalysis to have reached a peak intensity of 185 kt (~95 m s^{-1}) around 1200 UTC 23 October (Fig. 9) while centered about 130 n mi (~241 km) southwest of Manzanillo, Mexico. The analyzed peak intensity was influenced by estimates from the advanced Dvorak technique (ADT; Olander and Velden 2007). A reprocessing of Patricia with the latest version of the ADT (which includes reconnaissance calibration) recorded the highest-ever ADT T number (T8.4) for any TC during the geostationary satellite era (since circa 1979) regardless of basin (Velden et al. 2017). The NHC best track makes Patricia the strongest hurricane on record globally (Table 1).

Patricia reached the western periphery of the midlevel ridge centered over the Gulf of Mexico around this time and turned north-northwestward and northward while maintaining its intensity. By the time the last aircraft missions reached Patricia around 1800 UTC 23 October, the hurricane had turned north-northeastward with some increase in forward speed in response to a mid-/upper-level short-wave trough moving across Baja

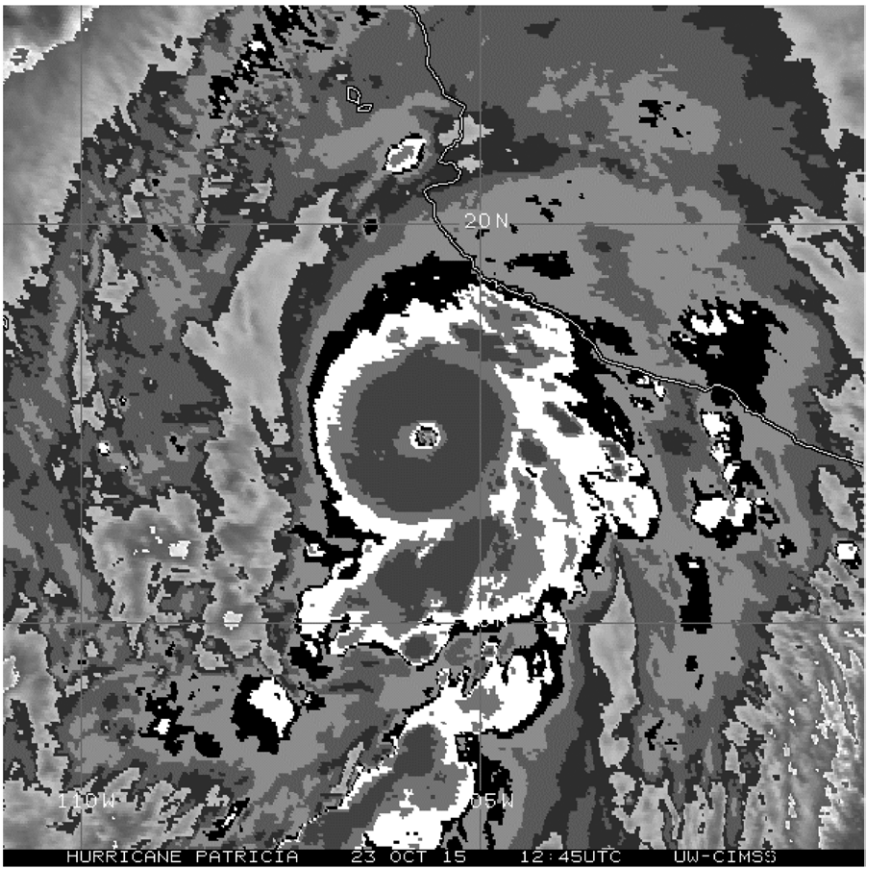

Fig. 9. GOES enhanced infrared image valid 1245 UTC 23 Oct, when Patricia had the highest ADT estimate on record.

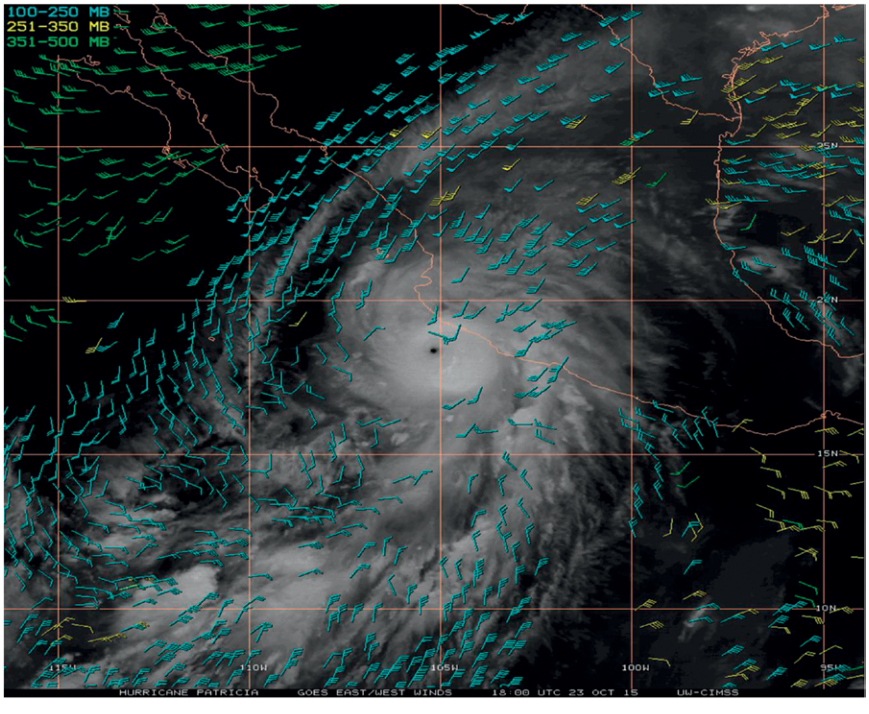

Fig. 10. As in Fig. 6, but for 1800 UTC 23 Oct.

California and northwestern Mexico (Fig. 10). Although the WP-3D aircraft still found surface wind speed near 180 kt (~93 m s^{-1}) on its first pass through Patricia in the southeastern quadrant, a 2027 UTC 23 October passive microwave satellite overpass (Fig. 11) indicated a distinct double eyewall structure, suggestive of an imminent weakening trend. Upper-air and SHIPS analyses also indicated that southwesterly vertical wind shear was increasing over the TC (cf. Fig. 4) and a final pass by the WP-3D around 2030 UTC indicated that a rapid filling had begun; the peak flight-level wind speed had decreased nearly 50 kt (~26 m s^{-1}) in the same quadrant traversed earlier and the central pressure had risen 24 hPa in the 3 h since the previous fix.

Patricia continued to rapidly weaken before landfall and reached the southwestern coast of Mexico in the state of Jalisco, near Playa Cuixmala, around 2300 UTC 23 October, as a category 4 hurricane on the Saffir–Simpson hurricane wind scale, with an estimated intensity of 130 kt (~67 m s^{-1}) and a minimum pressure of around 932 hPa. Patricia's central pressure is estimated to have risen 54 hPa in the 5 h prior to landfall, the highest overwater filling rate in either the Atlantic or eastern North Pacific historical record (cf. Table 1). The hurricane continued to weaken rapidly while it moved over the high terrain of the Sierra Madre, and Patricia fell below hurricane intensity before passing well to the west of Guadalajara around 0300 UTC 24 October. When the midlevel center raced northeastward and separated from the low-level center overnight, Patricia weakened to a tropical depression and then dissipated later the next morning over central Mexico, though the system later dropped up to 60.53 mm of rain near Powell, Texas, and spawned a tornado near Houston.

OBSERVATIONS OF PATRICIA'S LIFE CYCLE. *Kinematic and precipitation structure and evolution during rapid intensity changes.* The sequence of GOES visible images in Fig. 2 illustrates the extremely rapid development and small size of Patricia. In the span of approximately 72 h, Patricia progressed from a developing circulation with vigorous asymmetric convection to a small CDO with a pinhole eye. The subsequent weakening phase was equally impressive, beginning just before landfall on the Mexican coast, with the satellite presentation (not shown) rapidly deteriorating as Patricia encountered high vertical wind shear and a secondary eyewall formed, and later as Patricia interacted with the mountainous terrain after landfall.

Figure 12 shows individual, representative reflectivity sweeps of the WP-3D lower-fuselage radar during its three missions. An area of high reflectivity that may have been associated with a developing eyewall was seen to the south and southeast of the center at 2042 UTC 21 October, with another band of high reflectivity to the north and northwest. By 1856 UTC 22 October, Patricia showed a compact eye and high-reflectivity eyewall, with a notable lack of reflectivity on the northwest side outside the eyewall, and a broad shield of moderate reflectivity to the east and south. During the next mission an even smaller eye, with a diameter ~15–20 km, was seen. Also noteworthy is the appearance of a concentric ring of high reflectivity ~60 km from the center. This likely was the secondary eyewall that had developed, as revealed by microwave imagery (cf. Fig. 11).

Figure 13 shows the kinematic and precipitation structure on 21 October, when Patricia began to intensify rapidly. Patricia had a distinct circulation at 8-km altitude displaced ~25 km to the west-southwest of the 2-km-altitude circulation center (Fig. 13a). Such a displacement is consistent with the easterly shear that Patricia was experiencing south of the midlevel ridge in the Gulf of Mexico. The height of the 20-dB*Z* echo tops was a maximum on the southwest (i.e., downshear) side where echo tops in excess of 14 km were consistent with the core of high reflectivity seen in the lower fuselage image in

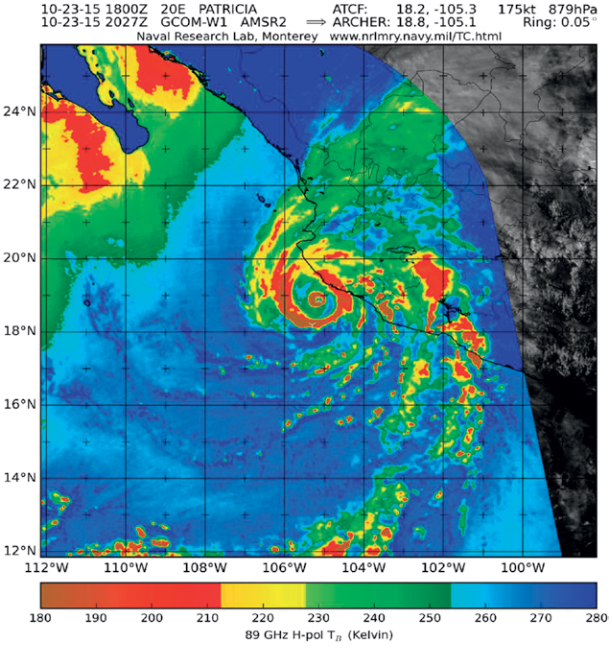

Fig. 11. Advanced Microwave Scanning Radiometer 2 (AMSR-2) 89-GHz brightness temperature at 2027 UTC 23 Oct, depicting concentric eyewalls just before landfall. (Figure courtesy Josh Cossuth and NRL Monterey TC web page team.)

Fig. 12a. These high echo tops, indicative of deep convection, were located at and inside the radius of maximum wind speed (RMW) at 2-km altitude, a location often associated with intensifying TCs (e.g., Rogers et al. 2013b, 2015, 2016; Stevenson et al. 2014; Susca-Lopata et al. 2015).

Analyses of horizontal wind velocity from Doppler radar data (Reasor et al. 2009) were produced on a three-dimensional grid with 1.5-km horizontal and 0.5-km vertical spacing (Fig. 14). This horizontal resolution, higher than the typical horizontal resolution of 2 km (e.g., Rogers et al. 2012), was used because of the extraordinarily small size of Patricia. A wind speed

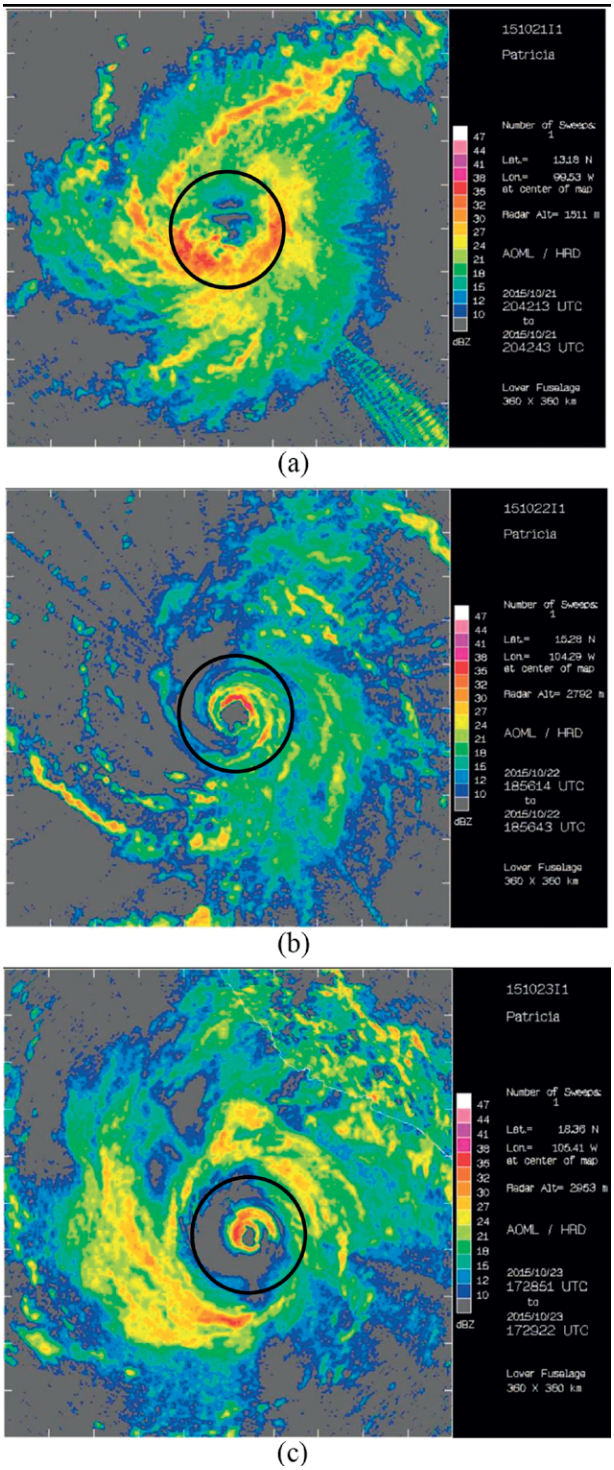

Fig. 12. WP-3D lower fuselage reflectivity at ~1.5-km altitude (21 Oct) and ~2.8 km (22–23 Oct). Domains are 360 km on a side. Circle denotes 50 km range ring.

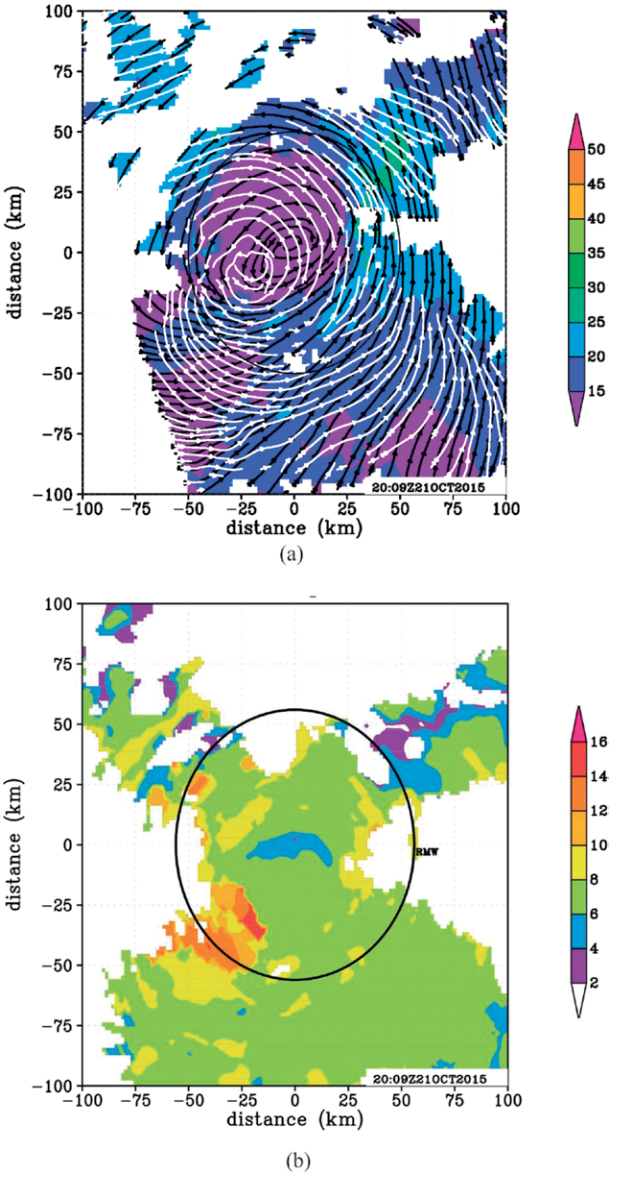

Fig. 13. (a) Earth-relative wind speed at 2-km altitude (shaded, m s^{-1}) and streamlines of storm-relative flow at 2 km (black) and 8 km (white) during WP-3D mission on 21 Oct; (b) height of 20-dBZ echo top (shaded, km) during same mission. Black circle in (b) denotes location of azimuthally averaged radius of maximum 2-km winds.

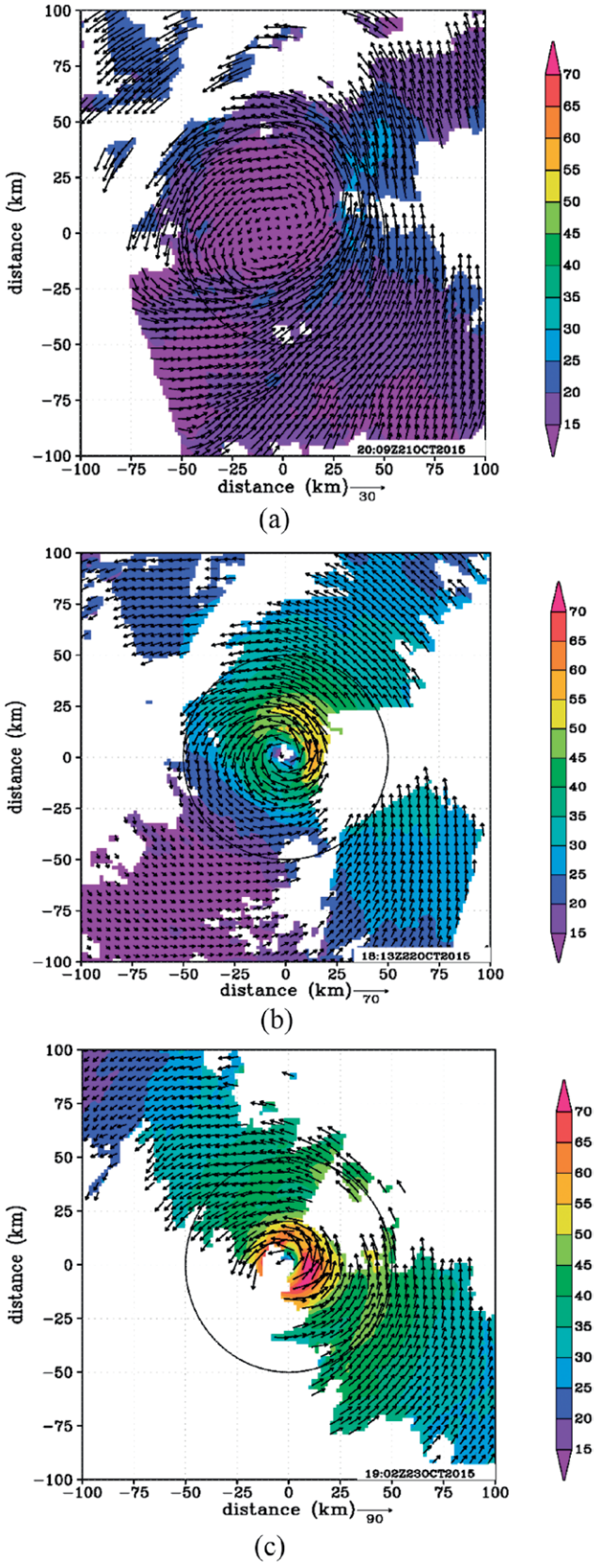

Fig. 14. Earth-relative wind speed (shaded, m s^{-1}) and wind vectors at 2-km altitude for 21–23 Oct. Circle denotes 50-km-range ring.

maximum of ~25 m s^{-1} at ~50-km radius was seen on the southeast side of Patricia on 21 October, consistent with the location of the reflectivity maximum shown in Fig. 11. On 22 October, the wind speed increased to ~50 m s^{-1}, and the RMW had contracted to a radius of ~20 km. By 23 October, the maximum wind speed exceeded 70 m s^{-1} at a radius of ~10 km. This is less than the peak flight-level and SFMR wind speeds, but this likely reflects the limitations of capturing these structures, and their extreme gradients, on a 1.5-km grid. A broad wind field was seen outside the RMW on this pass, with some indication of a secondary wind speed maximum at about 40–50-km radius from the center, roughly consistent with the location of the outer reflectivity maximum shown in Fig. 12.

The sequence of wind speed swaths from HIRAD (Fig. 15) similarly shows the dramatic tightening and intensification of Patricia. HIRAD is not sensitive to wind speed less than about 15–20 m s^{-1}, but a region of weak wind representing the TC center about 80 km across was seen on the afternoon of 21 October. The HIRAD wind speed appeared to be high biased relative to the HDSS dropsonde wind measurements on this day, but not on the others. By the next afternoon, the eye had contracted and the RMW was about 15 km, with the radius of hurricane-force winds extending to 26 km. By the 23 October flight, the RMW from HIRAD varied between about 8 and 12 km, depending on the quadrant. Despite the extreme intensity (76 m s^{-1} peak wind speed at 12-km radius in the south-southwest eyewall), hurricane-force winds only extended 29 km from the center, as retrieved by HIRAD.

Dropsonde measurements from the low-altitude aircraft (i.e., WP-3D, C-130) showed the unique nature of Patricia in the lower troposphere. Stern et al. (2016), examining dropsondes released in TCs since 1997, found that low-level updrafts >10 m s^{-1} are ubiquitous within very intense TCs and nearly nonexistent in weaker ones. Twenty-nine dropsondes were released in the eye and eyewall from the WP-3D and C-130 aircraft. One dropsonde, released 1734 UTC 23 October in the southern eyewall (not shown), reported a maximum horizontal wind speed of 98.3 m s^{-1} at an altitude of 791 hPa, making this the eleventh fastest horizontal wind measured by dropsonde in a TC. Another dropsonde rose more than 1 km in a very strong updraft starting immediately after release in the southeastern eyewall, but the

instrument failed while still rising about 4 min after its deployment. The maximum updraft measured was 27.4 m s^{-1}, which is ~3 m s^{-1} higher than the largest updraft previously measured by dropsonde (Stern et al. 2016) and nearly the same magnitude as the strongest low-level in situ measurement of an updraft in a TC (Aberson et al. 2017). The instrument rotated into the northern eyewall, almost 180° around the vortex, before it stopped reporting. The sounding was nearly saturated throughout, and the equivalent potential temperature was measured between 374 and 378 K—very high values for the region between 3- and 4-km altitude. No strong downdrafts >10 m s^{-1} were measured by the WP-3D or C-130 dropsondes in Patricia.

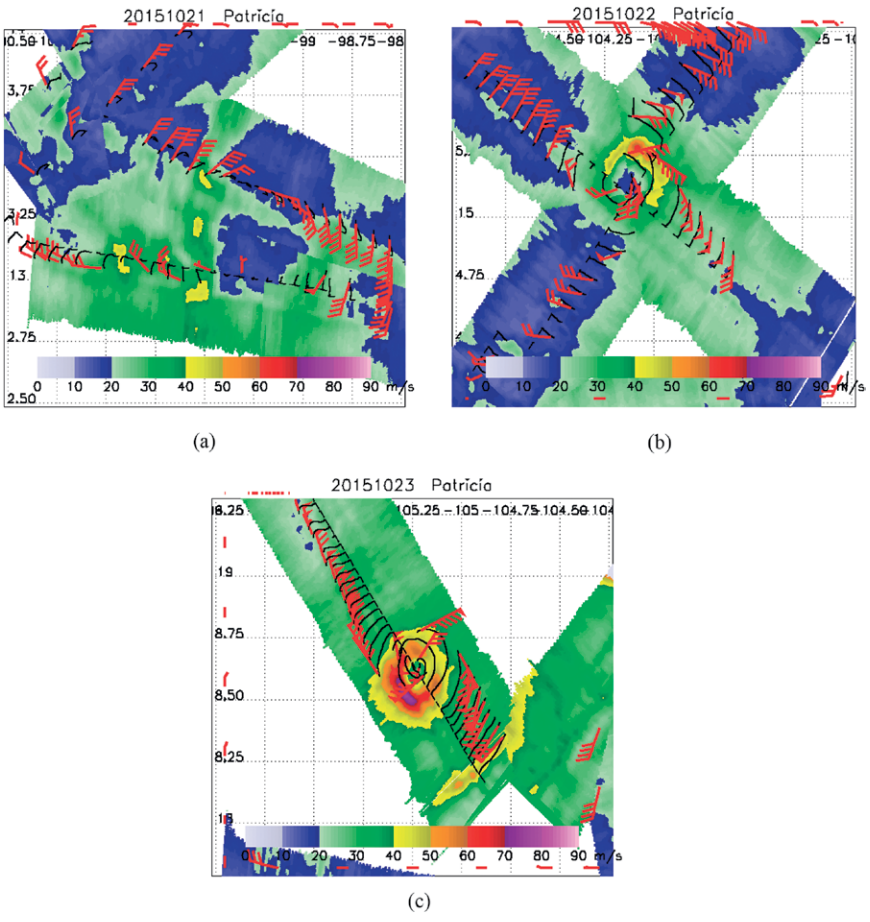

Fig. 15. HIRAD surface wind speeds (shaded, m s^{-1}), with HDSS dropsonde trajectories and near-surface winds (barbs, m s^{-1}), derived following Uhlhorn et al. (2007). Flag denotes wind speeds ~25 m s^{-1}; full barb denotes wind speeds ~5 m s^{-1}; half barb denotes wind speeds ~2.5 m s^{-1}. (a) 1956 UTC 21 Oct, (b) 1823 and 1906 UTC 22 Oct, and (c) 2001 UTC 23 Oct.

Radius–height plots of azimuthally averaged reflectivity and tangential wind speed for the three missions are shown in Fig. 15. A broad wind field was seen on 21 October (Fig. 16a). The peak azimuthally averaged tangential wind speed at 2-km altitude, estimated at ~20 m s^{-1}, was located at ~50–55-km radius from the center. Little vertical extent to the reflectivity was apparent, except for a region above 10 km at a similar radius to the broad wind speed maximum. A considerable difference was apparent by 22 October (Fig. 16b). Azimuthally averaged tangential wind speed in excess of 45 m s^{-1} was located at ~15–20-km radius from the center. A clear eyewall had developed, as strong tangential wind and high reflectivity extended above 14-km altitude. Outside the eyewall, high reflectivity did not extend above the freezing level at ~5-km altitude, while the tangential wind speed showed a steady decrease with radius. By 23 October (Fig. 16c), Patricia was even smaller, with a peak tangential wind speed at ~10-km radius. The tangential wind speed maximum also showed an unusual peak >65 m s^{-1} between 3- and 6-km altitude. An analysis of the HDSS dropsondes from the WB-57 showed a similar elevated wind speed maximum [see Fig. 13 in Doyle et al. (2017)], suggesting that it was real. A similar elevated wind speed maximum was also observed in Hurricane Gloria (Franklin et al. 1993). Extremely high azimuthally averaged reflectivity was associated with this inner eyewall as well. A clear secondary wind speed maximum was also apparent between 40 and 50 km from the center and was consistent with the secondary wind speed maximum at 2 km shown in Fig. 14c. The highest reflectivity sloped outward with height along the outer edge of this secondary wind speed maximum, which likely explained why the outer reflectivity maximum seen at 60-km radius in Fig. 12c (cf. discussion above) was farther from the center than that at 2-km altitude seen in Fig. 14c.

Combining the deep-layer kinematic and thermodynamic observations collected in Patricia,

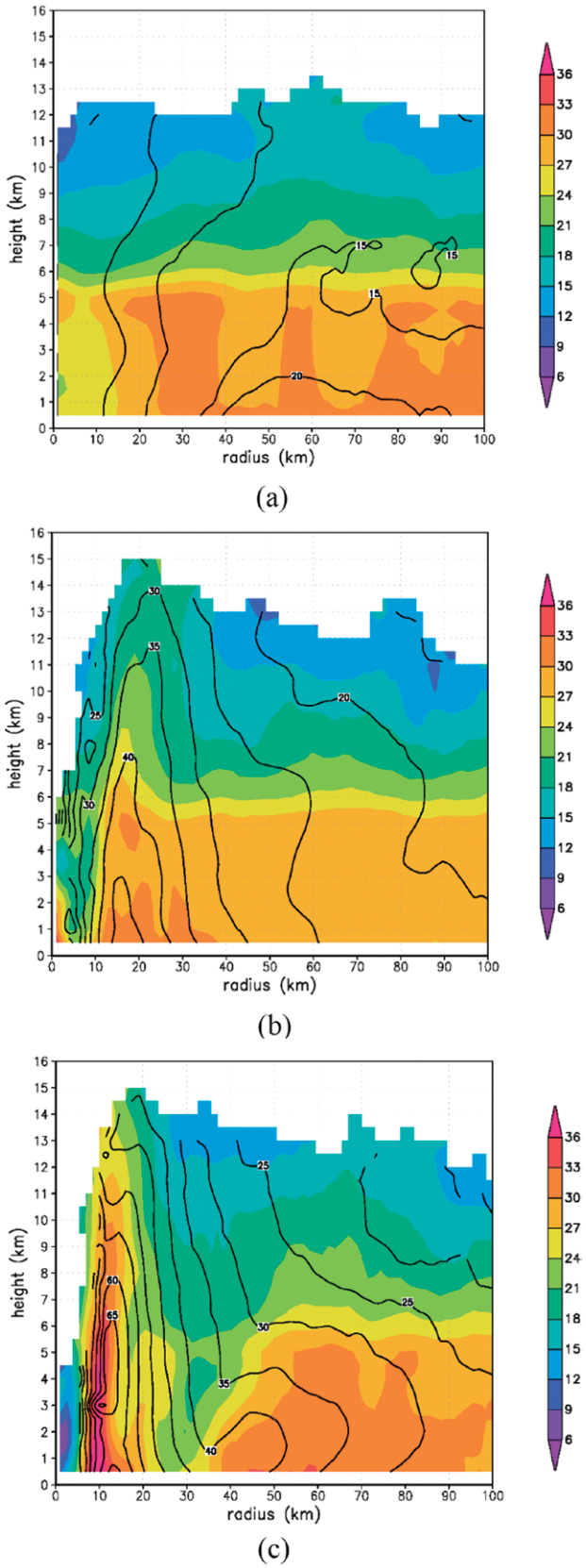

Fig. 16. Azimuthally averaged reflectivity (shaded, dBZ) and tangential wind (contour, m s^{-1}) for (a) 2009 UTC 21 Oct, (b) 1813 UTC 22 Oct, and (c) 1902 UTC 23 Oct.

Fig. 17 shows the azimuthally averaged secondary circulation and potential temperature derived from the tail Doppler radar and dropsondes on 22 October using a Spline Analysis at Mesoscale Utilizing Radar and Aircraft Instrumentation (SAMURAI; Bell et al. 2012). The secondary circulation revealed inflow at low levels converging in the eyewall into a deep updraft and upper-level outflow. A downdraft originating from upper levels cascaded down the inner edge of the eyewall and turned to outflow at low levels. The potential temperature structure was consistent with the secondary circulation, indicating lowered isentropes in the eye associated with deep subsidence.

Warm-core structure and surface wind near peak intensity. The WB-57 flight track crossed over the core of Patricia twice during its mission on 22 October and once the next day, just after peak intensity (cf. Fig. 2). Analysis of the quality-controlled high-resolution HDSS dropsondes (Bell et al. 2016) reveals that Patricia had a notable warm-core structure both days (Fig. 18). The anomaly was calculated by taking the difference between selected dropsonde temperature profiles (including the eye sounding) along the WB-57 transect and a reference environmental sounding. The choice of a representative environmental sounding to use in calculating the thermal perturbation analyses is varied in the literature. LaSeur and Hawkins (1963) and Hawkins and Rubsam (1968) used a climatological reference state, the annual mean sounding of Jordan (1958) (i.e., not the hurricane-season sounding). Halverson et al. (2006) used a local reference state, and Durden (2013) used both climatological and local (surface-based radiosondes at the same location) reference states. Stern and Zhang (2016) used the Dunion tropical sounding (Dunion 2011) and a local reference state from aircraft dropsondes. To be consistent with the early studies and for historical perspective, the Jordan annual mean profile was used for the environmental sounding and the warm-core analyses presented in Fig. 18. This anomaly should be interpreted relative to a climatological framework and not as an absolute temperature perturbation in Patricia. For interest, the warm anomaly peak using a local mean of environmental soundings was 18.6°C [further details on the HDSS thermal anomaly analyses are described in D. Herndon and C. Velden (2017, manuscript submitted to *J. Appl. Meteor. Climatol.*)]. Table 2 lists values of warm-core anomaly

for the TCs mentioned above, including the reference state used in the calculation and the citation for these studies.

On 22 October, several temperature maxima were indicated in the cross section (Fig. 18a), with the strongest (14.9°C) near 250–300 hPa. By 23 October, when Patricia was near peak intensity, two maxima were indicated near 300–350 and 550–600 hPa (Fig. 18b), with the strongest peak (21.7°C) near 600 hPa. For comparison, the cross section of Hurricane Inez (1966) as reported in Hawkins and Imbembo (1976, their Fig. 6) also showed two maxima (near 300 and 650 hPa), but with much weaker magnitude (peak of ~9°C at both levels). However it should be emphasized that large portions of the Inez cross-sectional analysis were interpolated between aircraft flight-level measurements. The high-resolution HDSS profiles during Patricia offered an unprecedented detailed three-dimensional sampling of a full-troposphere TC warm core. From the analysis of the dropsondes, and as indicated in Table 2, the case can be made that Patricia had the largest-ever observed TC warm-core anomaly.

The combination of the HIRAD wind swath and the HDSS fall trajectories and surface wind speeds on 23 October shown in Fig. 19 provides particularly useful context for the dropsonde measurements. Since dropsondes are single-point measurements, it is virtually impossible for them to resolve the peak wind speed in Patricia's tight circulation, even though they are released every 20 s (4 km). None of the dropsondes fell into the region where HIRAD indicates the strongest surface wind speed in the southwestern quadrant of the tiny eyewall. The SFMR on the NOAA WP-3D measured peak wind speed along its flight track (in the southeastern quadrant) of 93 m s^{-1} at 1733 UTC, then 67 m s^{-1} at 2033 UTC. HIRAD retrieved a peak wind speed about 10 km to the left of the flight track, 76 m s^{-1} at 2001 UTC. One dropsonde stopped sending data while falling into that southwestern quadrant, where HIRAD depicts the strongest wind and the WP-3D radar depicted the highest reflectivity, with a short spiral band connecting to the inner eyewall. In other quadrants, most dropsondes splashed radially inward or outward of the sharply peaked RMW. Two dropsondes

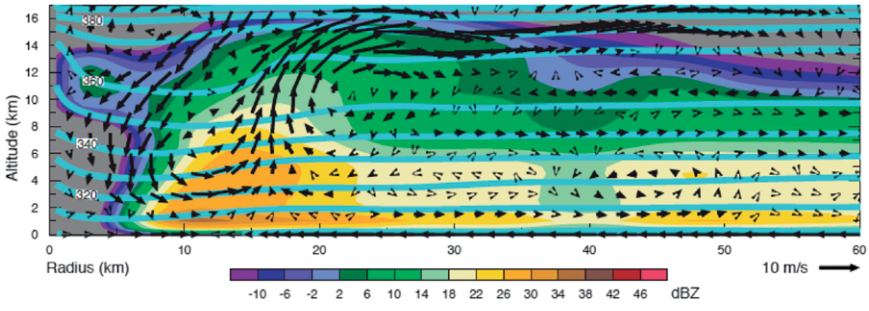

Fig. 17. SAMURAI axisymmetric variational analysis of radar reflectivity (color, dBZ), potential temperature (cyan contours, 10-K increments), and secondary circulation (vectors) at 1800 UTC 22 Oct.

Table 2. The peak magnitudes of TC warm-core anomalies from past and current studies. The reference states used to calculate the anomalies are also noted. "Local" refers to a reference state based on soundings nearby either in time or location.

Tropical cyclone name and year	Peak anomaly (°C)	Reference state used	Citation
Cleo (1964)	11.0	Jordan (1958) sounding	LaSeur and Hawkins (1963)
Hilda (1964)	16.0	Jordan (1958) sounding	Hawkins and Rubsam (1968)
Inez (1966)	9.0	Jordan (1958) sounding	Hawkins and Imbembo (1976)
Flo (1990)	~18.0	Local	Durden (2013)
Erin (2001)	11.0	Local	Halverson et al. (2006)
Earl (2010)	~17.0	Local	Durden (2013)
Earl (2010)	~17.0	Dunion (2011) tropical sounding	Stern and Zhang (2016)
Earl (2010)	~13.0	Local	Stern and Zhang (2016)
Patricia (2015)	21.7	Jordan (1958) sounding	Rogers et al. (2017)
Patricia (2015)	18.6	Local	D. Herndon and C. Velden (2017, manuscript submitted to *J. Appl. Meteor. Climatol.*)

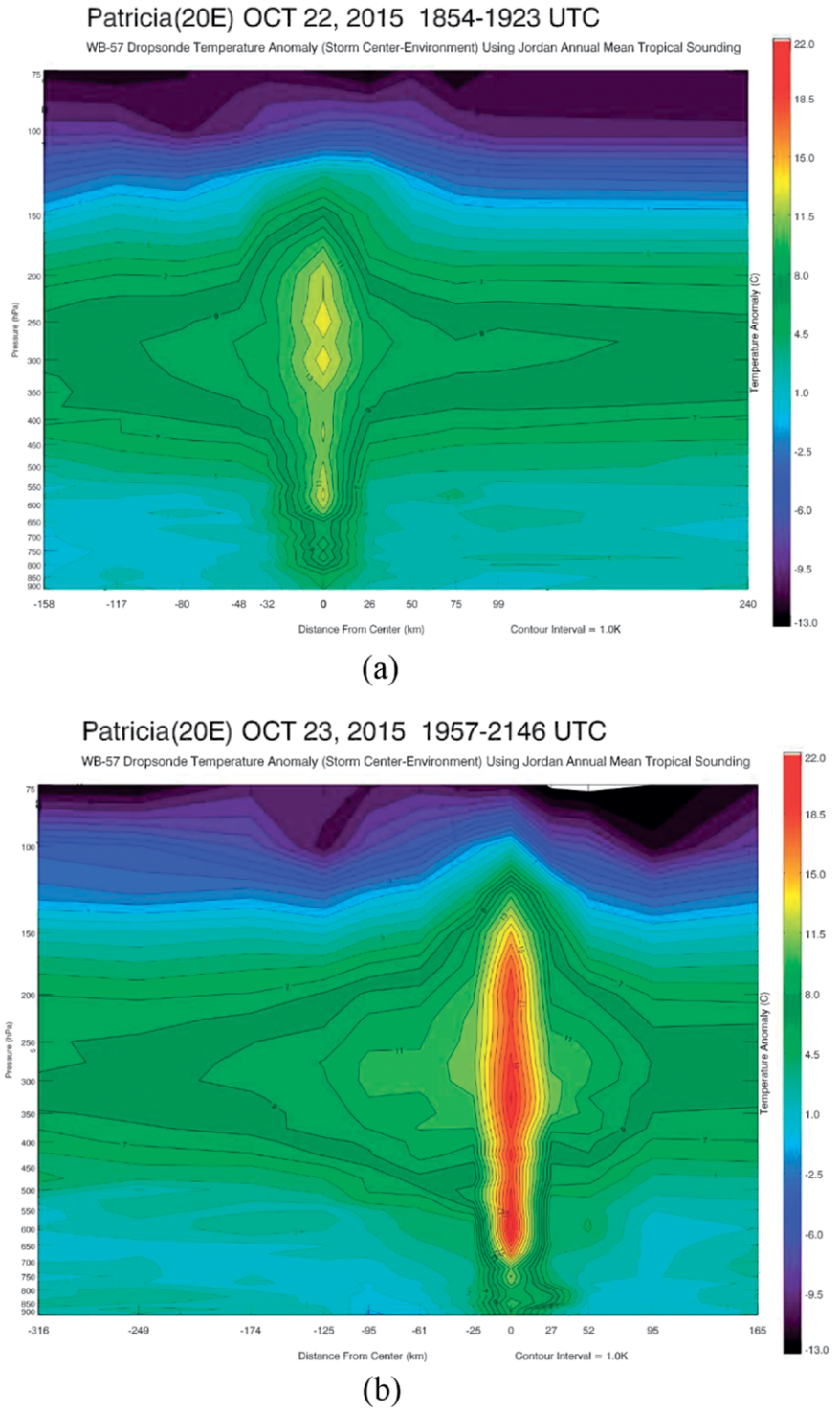

Fig. 18. Patricia warm-core anomaly (1.0°C intervals) derived from selected HDSS soundings along WB-57 core overflight transects and departure from the Jordan annual mean tropical sounding, centered at (a) 1854–1923 UTC 22 Oct and (b) 1957–2146 UTC 23 Oct 2015. Here the *x* axis in (a) is along the transect in Fig. 2c from (left) northwest to (right) southeast, while in (b) it is along the transect in Fig. 2d from (left) southwest to (right) northeast. The values below the *x* axis indicate dropsonde locations (in km from storm center) for profiles used to construct the cross sections through Patricia. [Figure from D. Herndon and C. Velden (2017, manuscript submitted to *J. Appl. Meteor. Climatol.*).]

released in the eye reported near-surface wind speeds of 11 and 35 m s^{-1}, only 4 km apart. Surface pressures from those dropsondes were 905 and 909 hPa, respectively.

Rapid weakening and landfall. Equally as remarkable as the rapid intensification of Patricia was its rapid weakening just prior to and after landfall on the Mexican coast. A WB-57 high-density dropsonde sequence was coincident with a WP-3D eyewall penetration just before the hurricane made landfall. A SAMURAI analysis of the structure at this time (Fig. 20) indicates that Patricia had begun to feel the effects of increasing southwesterly vertical shear and the developing secondary eyewall. The analysis shows a rotation in the azimuthal location of the wind speed maximum with height, with an 80 m s^{-1} maximum 13 km from the center in the southwest quadrant at 2-km height (Fig. 20a) switching to a 70-m s^{-1} maximum in the northeast quadrant at 6-km height (Fig. 20b). The secondary maxima in the wind speed and reflectivity are evident at large radii from the center, indicative of a developing secondary eyewall that also contributed to weakening. The HDSS dropsondes were deployed across the primary eyewall (Fig. 20c) and followed the swirling flow as they fell from the stratosphere. Despite the tiny target, one HDSS dropsonde managed to fall nearly vertically in

the calm wind in the eye, yielding a full-tropospheric eye sounding just after maximum intensity (Fig. 20d). A deep-layer inversion was evident at low levels with the temperature exceeding 20°C at 600 hPa, and a very high tropopause is found at 100 hPa.

Landfall occurred in the Mexican state of Jalisco, very close to Emiliano Zapata, at 2300 UTC 23 October (Fig. 21; Morgerman 2015). Despite the rapid weakening leading up to landfall—and despite the apparent development of a secondary eyewall as seen on reconnaissance radar—surface data and observations collected by the iCyclone team from the landfall point suggest the TC retained a narrow, compact core. A detailed chronology of events was created using continuous time-stamped video footage shot during the passage of the hurricane. Based on this chronology, damaging winds only persisted for ~2 h in Emiliano Zapata—from ~2225 to 0030 UTC—suggesting they were confined very close to the TC's center. The most violent winds, strong enough to inflict significant structural damage to the hotel from which the data were collected, immediately followed the brief calm of the eye and only lasted ~17 min. There was no observed secondary wind speed maximum at this location.[2] Despite the short duration of significant winds, damage was heavy, including almost 100% defoliation of trees (leaving jungle hills stripped clean of vegetation), snapped palm trees, crumpled communications towers, broken concrete power poles, and major damage to houses and buildings (Fig. 22).

A minimum pressure of 937.8 hPa was measured by the iCyclone team in Emiliano Zapata at 2312 UTC, during a short lull as the edge of the eye passed over (cf. Fig. 21). This reading is further evidence the TC filled rapidly leading up to landfall. However, air-pressure data sampled every minute from two barometers in the hotel room at the iCyclone observation site suggest the TC retained an extremely steep pressure gradient. Crude calculations using i) pressure change over time and ii) the TC's forward speed suggest gradients over 10 hPa (n mi)$^{-1}$ (~5.4 hPa km^{-1})—in one place as high as 11.4 hPa (n mi)$^{-1}$ (~6.2 hPa km^{-1}). These peak gradients were observed in the south eyewall, during the short period of especially violent winds, as the TC moved away and the pressure was rapidly rising. These surface observations and data from Emiliano Zapata suggest that, despite prelandfall filling, Patricia's wind core—and RMW—did not dramatically expand as it weakened.

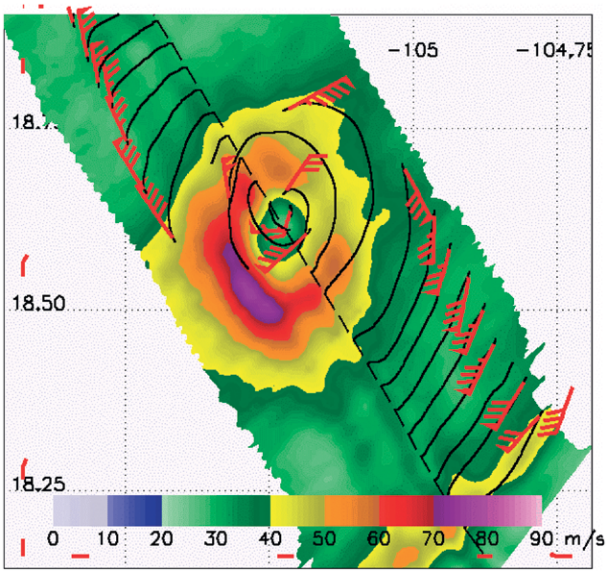

Fig. 19. As in Fig. 15c, but zoomed in on the center for 23 Oct.

SUMMARY AND CONCLUDING REMARKS. Hurricane Patricia rewrote the TC record books with a historical rate of intensification, peak intensity, and rate of overwater weakening, among other parameters. A favorable environment, marked by dual outflow channels, low vertical wind shear, a moist and unstable atmosphere, and anomalously warm water with a deep oceanic mixed layer, combined to allow Patricia to deepen to an extremely intense hurricane with a very small core. Patricia evolved from a tilted structure with deep convection on its southwest side inside the RMW to a vertically aligned circulation with a solid eyewall of heavy precipitation forming a small core. The eyewall was characterized by a high tropopause and subsidence along the inner edge. On the day of peak intensity (23 October), a warm-core anomaly of 21.7°C departure from the Jordan annual mean tropical sounding was observed near 600 hPa from high-resolution dropsonde data, which may be the largest thermal perturbation ever observed in a TC. The surface wind speed was measured at close to 175 kt (~90 m s^{-1}) during this time, and dropsondes measured extremely strong horizontal wind speeds above the surface and encountered the strongest dropsonde-measured updraft in a TC on record. Just prior to landfall, the small core showed a rotation of the wind speed with height, likely in response to increasing vertical shear, and the storm also developed a sec-

[2] It is important to note that this as well as other wind observations at this location are subjective; there unfortunately was not an anemometer at this location.

ondary wind speed maximum. As quickly as Patricia intensified, it weakened prior to landfall and continued this rapid weakening after landfall. In situ pressure observations at landfall showed that the central pressure had risen dramatically from peak intensity. However, these observations also showed the TC retained an extremely steep pressure gradient around the eye—and surface observations and damage showed the TC retained a narrow, compact core of violent winds.

Like so many cases of rapid intensity change (Marks and Shay 1998; Rogers et al. 2006), the processes and structures responsible for Patricia's intensification (e.g., vertical wind shear, atmospheric stability, SST and OHC, upper-level outflow channels, vortex size and alignment, and distribution and intensity of deep convection) spanned a multitude of spatial and temporal scales. One challenge in predicting such rapid intensity changes is in accurately depicting these processes and the

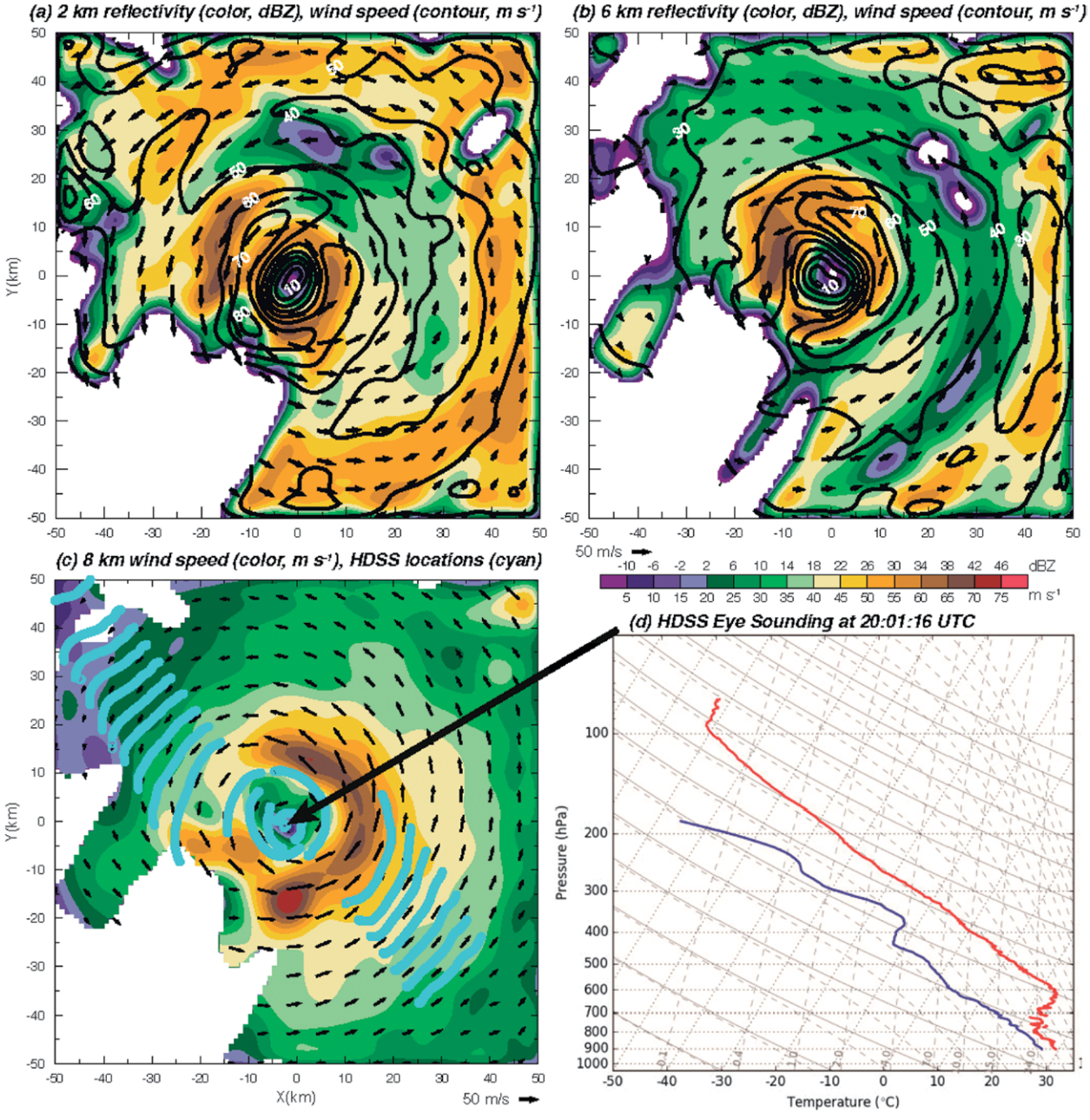

Fig. 20. SAMURAI variational analysis 2100 UTC 23 Oct of radar reflectivity (color, dBZ) and storm-relative wind speed (10 m s^{-1}, contours) and wind vectors at (a) 2 km and (b) 6 km and (c) wind speed at 8 km with HDSS dropsonde trajectories (blue lines). (d) Skew *T*–log*p* eye sounding of temperature (red) and dewpoint (blue) at 2001:16 UTC at location indicated in (c) by the arrow.

interactions within and across scales. This challenge was acute in the case of Patricia, as the storm was extremely small and could not be well depicted using a numerical model grid with a 2–3-km grid spacing. Predicting a rare event like Patricia is inherently difficult, and this is even moreso when the processes at least partially responsible for the intensification (e.g., deep convection) have predictability constraints (e.g., Zhang and Sippel 2009; Judt and Chen 2016), suggesting probabilistic approaches to prediction may be the best approach for intensity forecasts.

Despite the challenges inherent to improving prediction of such extreme events, the combination of high-altitude dropsondes, wide-swath surface wind speeds, airborne Doppler measurements, and in situ pressure measurements at and after landfall provide a unique opportunity to study Patricia's structure and evolution during its unprecedented intensity changes. Research that can be expected from these datasets include, but are certainly not limited to, studies on mechanisms responsible for the formation and structure of the warm core during the intensification and peak intensity stages, the role of upper-level outflow on the evolution of the system, boundary layer kinematic and thermodynamic structure and its role in convective-scale structure and storm intensification, and the assimilation of these high-density datasets into numerical models. With a better understanding of these and other processes during Patricia's life cycle, the potential exists to develop and improve the forecasting

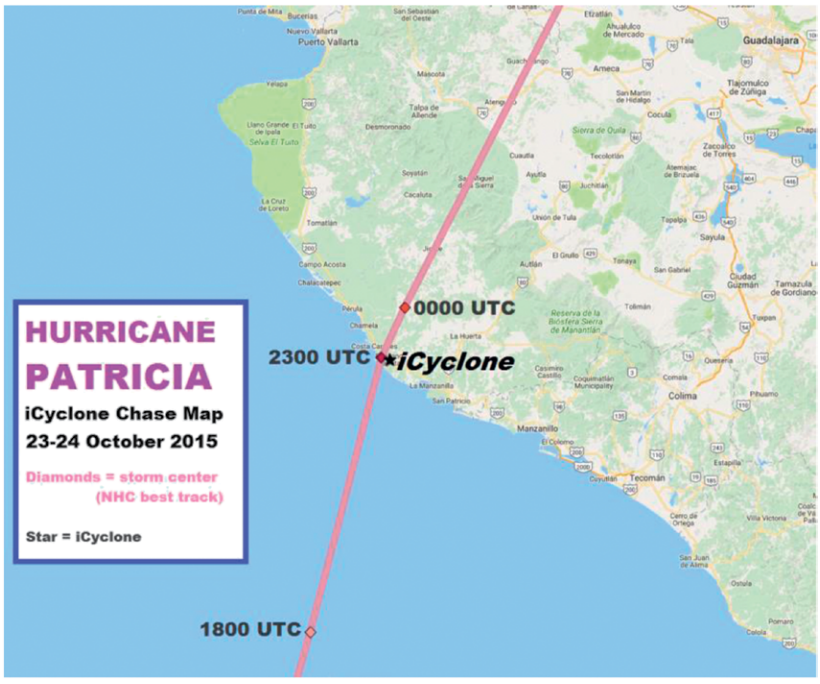

(a)

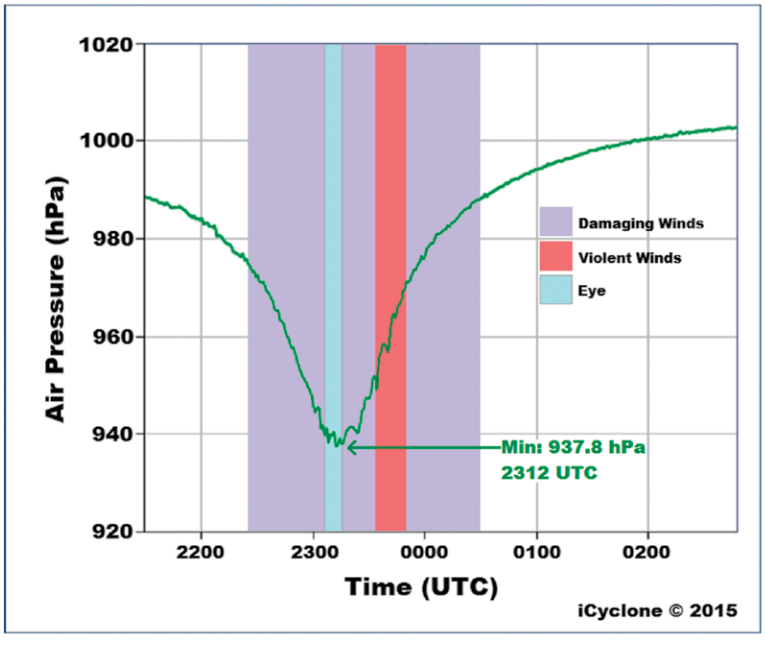

HURRICANE PATRICIA: 23-34 Oct 2015
Emiliano Zapata, Jalisco, Mexico
19.38973N 104.96391W – ref el ~18 m

(b)

Fig. 21. (a) Track of Patricia at landfall and location of iCyclone team; (b) barogram from iCyclone team during eye passage. Periods of eye passage and strongest winds indicated. "Damaging" winds are those that can tear large branches from trees; "violent" winds are those inflicting significant structural damage.

systems required to better predict these extraordinary events.

ACKNOWLEDGMENTS. We acknowledge the flight and ground crews from NOAA, NASA, and the Air Force for collecting the WP-3D, WB-57, and C-130 data. RFR and SDA acknowledge the support of NOAA base funds. JDD acknowledges the support of the Office of Naval Research's (ONR) Program Elements (PEs) 0601153N and 0602435N, as well as the National Oceanic and Atmospheric Administration (NOAA) sponsored Hurricane Forecast Improvement Project (HFIP). JDD acknowledges support for computational resources through a grant of Department of Defense High Performance Computing time from the DoD Supercomputing Resource Center at Stennis, Mississippi. DJC and CSV acknowledge the support of the ONR Tropical Cyclone Intensity project. MMB acknowledges support by Office of Naval Research Award N000141410118. Thanks to Derrick Herndon (CIMSS) for reproducing Fig. 17. LKS gratefully acknowledges a grant from the NASA Physical Oceanography Program (Grant NNX15AG43G). We are grateful to Ms. Jodi Brewster (RSMAS) who provided the ocean figures used in this paper. The Naval Oceanographic Office provides the daily altimeter data from multiple missions that includes quality control and error reduction and generates the daily SSHA products operationally at NOAA NESDIS. The NOAA GEO-Polar SSTs are provided by NESDIS. Our thanks also go to Chris Landsea (NHC), two anonymous reviewers, Eric Blake and Michael Brennan (both from NHC), and Dan Stern (NRL) for their helpful comments, and John Kaplan (NOAA HRD) and Jon Zawislak (Florida International University/CIMAS/HRD) for providing the diagnostics and interpretation of SHIPS data.

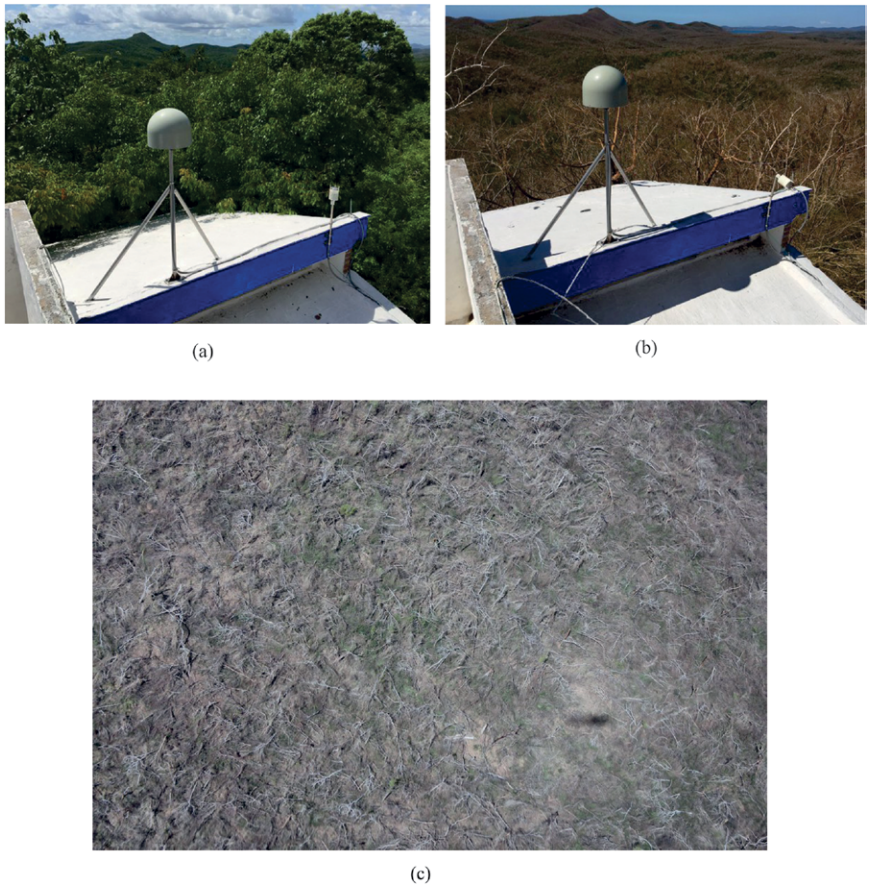

Fig. 22. (a) Before and (b) after damage photo at the Chamela Biosphere site. (Image courtesy John Galetzka.) (c) Trees denuded and completely flattened by the strong winds in the eyewall of Hurricane Patricia as viewed from a helicopter. (Image courtesy of Humberto Hernández Peralta.)

REFERENCES

Aberson, S. D., J. A. Zhang, and K. Nuñez Ocasio, 2017: An extreme event in the eyewall of Hurricane Felix on 2 September 2007. *Mon. Wea. Rev.*, **145**, 2083–2092, doi:10.1175/MWR-D-16-0364.1.

Bell, M. M., M. T. Montgomery, and K. A. Emanuel, 2012: Air–sea enthalpy and momentum exchange at major hurricane wind speeds observed during CBLAST. *J. Atmos. Sci.*, **69**, 3197–3122, doi:10.1175/JAS-D-11-0276.1.

——, and Coauthors, 2016: ONR Tropical Cyclone Intensity 2015 NASA WB-57 HDSS Dropsonde Data, version 1.0. NCAR/UCAR/Earth Observing Laboratory, accessed 1 May 2016, doi:10.5065/D6KW5D8M.

Black, P. G., L. Harrison, M. Beaubien, R. Bluth, H. Jonsson, A. B. Penny, R. W. Smith, and J. D. Doyle, 2017: High Definition Sounding System (HDSS) for atmospheric profiling. *J. Atmos. Oceanic Technol.*, **34**, 777–796, doi:10.1175/JTECH-D-14-00210.1.

Cecil, D. J., and S. K. Biswas, 2017: Hurricane Imaging Radiometer (HIRAD) wind speed retrievals and validation using dropsondes. *J. Atmos. Oceanic Technol.*, doi:10.1175/JTECH-D-17-0031.1, in press

DeMaria, M., M. Mainelli, L. K. Shay, J. A. Knaff, and J. Kaplan, 2005: Further improvements to the Statistical Hurricane Intensity Prediction Scheme (SHIPS). *Wea. Forecasting*, **20**, 531–543, doi:10.1175/WAF862.1.

Doyle, J. D., and Coauthors, 2017: A view of tropical cyclones from above: The Tropical Cyclone Intensity (TCI) experiment. *Bull. Amer. Meteor. Soc.*, doi:10.1175/BAMS-D-16-0055.1, in press.

Dunion, J. P., 2011: Rewriting the Climatology of the Tropical North Atlantic and Caribbean Sea Atmosphere. *J. Climate*, **24**, 893–908, doi:10.1175/2010JCLI3496.1.

Durden, S. L., 2013: Observed Tropical Cyclone Eye Thermal Anomaly Profiles Extending above 300 hPa. *Mon. Wea. Rev.*, **141**, 4256–4268, doi:10.1175/MWR-D-13-00021.1.

Figa-Saldaña, J. J., J. J. W. Wilson, E. Attema, R. Gelsthorpe, M. R. Drinkwater, and A. Stoffelen, 2002: The advanced scatterometer (ASCAT) on the meteorological operational (MetOp) platform: A follow-on for European wind scatterometers. *Can. J. Rem. Sens.*, **28**, 404–412, doi:10.5589/m02-035.

Franklin, J. L., S. J. Lord, S. E. Feuer, and F. D. Marks Jr., 1993: The kinematic structure of Hurricane Gloria (1985) determined from nested analyses of dropwindsonde and Doppler radar data. *Mon. Wea. Rev.*, **121**, 2433–2451, doi:10.1175/1520-0493(1993)121<2433:TKSOHG>2.0.CO;2.

Halverson, J. B., J. Simpson, G. Heymsfield, H. Pierce, T. Hock, and L. Ritchie, 2006: Warm Core Structure of Hurricane Erin Diagnosed from High Altitude Dropsondes during CAMEX-4. *J. Atmos. Sci.*, **63**, 309–324, doi:10.1175/JAS3596.1.

Hawkins, H. F. and D. T. Rubsam, 1968: Hurricane Hilda, 1964. *Mon. Wea. Rev.*, **96**, 428–452, doi:10.1175/1520-0493(1968)096<0428:HH>2.0.CO;2.

——, and S. Imbembo, 1976: The structure of a small, intense hurricane—Inez 1966. *Mon. Wea. Rev.*, **104**, 418–442, doi:10.1175/1520-0493(1976)104<0418:TSOASI>2.0.CO;2.

Hoarau, K., 2000: Supertyphoon Forrest (1983): The overlooked record holder of intensification in 24, 36, and 48 h. *Wea. Forecasting*, **15**, 357–360, doi:10.1175/1520-0434(2000)015<0357:SFSTOR>2.0.CO;2.

Hock, T. F., and J. L. Franklin, 1999: The NCAR GPS dropwindsonde. *Bull. Amer. Meteor. Soc.*, **80**, 407–420, doi:10.1175/1520-0477(1999)080<0407:TNGD>2.0.CO;2.

Holbach, H. M., and M. A. Bourassa, 2014: The effects of gap-wind-induced vorticity, the monsoon trough, and the ITCZ on east Pacific tropical cyclogenesis. *Mon. Wea. Rev.*, **142**, 1312–1325, doi:10.1175/MWR-D-13-00218.1.

Hurd, W. E., 1929: Northers of the Gulf of Tehuantepec. *Mon. Wea. Rev.*, **57**, 192–194, doi:10.1175/1520-0493(1929)57<192:NOTGOT>2.0.CO;2.

Jaimes, B., L. K. Shay, and E. W. Uhlhorn, 2015: Enthalpy and momentum fluxes during Hurricane Earl relative to underlying ocean features. *Mon. Wea. Rev.*, **143**, 111–131, doi:10.1175/MWR-D-13-00277.1.

Jordan, C. L., 1958: Mean soundings for the West Indies area. *J. Meteor.*, **15**, 91–97, doi:10.1175/1520-0469(1958)015<0091:MSFTWI>2.0.CO;2.

Judt, F., and S. S. Chen, 2016: Predictability and dynamics of tropical cyclone rapid intensification deduced from high-resolution stochastic ensembles. *Mon. Wea. Rev.*, **144**, 4395–4420, doi:10.1175/MWR-D-15-0413.1.

Kaplan, J., M. DeMaria, and J. A. Knaff, 2010: A revised tropical cyclone rapid intensification index for the Atlantic and eastern North Pacific basins. *Wea. Forecasting*, **25**, 220–241, doi:10.1175/2009WAF2222280.1.

Kimberlain, T. B., E. S. Blake, and J. P. Cangialosi, 2015: Hurricane Patricia. National Hurricane Center Tropical Cyclone Rep. EP202015, 32 pp. [Available online at www.nhc.noaa.gov/data/tcr/EP202015_Patricia.pdf.]

Klotz, B. W., and E. W. Uhlhorn, 2014: Improved stepped frequency microwave radiometer tropical cyclone surface winds in heavy precipitation. *J. Atmos. Oceanic Technol.*, **31**, 2392–2408, doi:10.1175/JTECH-D-14-00028.1.

Knapp, K. R., M. C. Kruk, D. H. Levinson, H. J. Diamond, and C. J. Neumann, 2010: The International Best Track Archive for Climate Stewardship (IBTrACS): Unifying tropical cyclone data. *Bull. Amer. Meteor. Soc.*, **91**, 363–376, doi:10.1175/2009BAMS2755.1.

La Seur, N. E., and H. F. Hawkins, 1963: An analysis of Hurricane Cleo (1958) based on data from research reconnaissance aircraft. *Mon. Wea. Rev.*, **91**, 694–709, doi:10.1175/1520-0493(1963)091<0694:AAOHCB>2.3.CO;2.

Levine, A. S., 2012: The influence of gap wind events on the monsoon trough and implications for eastern North Pacific cyclogenesis. *30th Conf. on Hurricanes and Tropical Meteorology*, Ponte Vedra, FL, Amer. Meteor. Soc., 3C.3. [Available online at https://ams.confex.com/ams/30Hurricane/webprogram/Paper205381.html.]

Marks, F. D., and L. K. Shay, 1998: Landfalling tropical cyclones: Forecast problems and associated research opportunities. *Bull. Amer. Meteor. Soc.*, **79**, 305–323, doi:10.1175/1520-0477(1998)079<0305:LTCFPA>2.0.CO;2.

Maturi, E., A. Harris, J. Mittaz, C. Merchant, B. Potash, W. Meng, and J. Sapper, 2008: NOAA's sea surface temperature products from operational geostationary satellites. *Bull. Amer. Meteor. Soc.*, **89**, 1877–1888, doi:10.1175/2008BAMS2528.1.

McCaskill, C., L. K. Shay, J. K. Brewster, and P. C. Meyers, 2016: Development and assessment of the Systematically Merged Pacific Ocean Regional Temperature and Salinity (SPORTS) climatology for oceanic heat content estimations. *J. Atmos. Oceanic Technol.*, **33**, 2259–2272, doi:10.1175/JTECH-D-15-0168.1.

Morgerman, J., 2015: iCyclone chase report—PATRICIA 2015. iCyclone, 37 pp. [Available online at https://goo.gl/fQ4lW0.]

Olander, T. L., and C. S. Velden, 2007: The advanced Dvorak technique: Continued development of an objective scheme to estimate tropical cyclone intensity using geostationary infrared satellite imagery. *Wea. Forecasting*, **22**, 287–298, doi:10.1175/WAF975.1.

Reasor, P. D., M. D. Eastin, and J. F. Gamache, 2009: Rapidly intensifying Hurricane Guillermo (1997). Part I: Low-wavenumber structure and evolution. *Mon. Wea. Rev.*, **137**, 603–631, doi:10.1175/2008MWR2487.1.

Roemmich, D., and Coauthors, 2009: The Argo Program: Observing the global oceans with profiling floats. *Oceanography*, **22**, 34–43, doi:10.5670/oceanog.2009.36.

Rogers, R. F., and Coauthors, 2006: The Intensity Forecasting Experiment (IFEX): A NOAA multiyear field program for improving tropical cyclone intensity forecasts. *Bull. Amer. Meteor. Soc.*, **87**, 1523–1537, doi:10.1175/BAMS-87-11-1523.

——, S. Lorsolo, P. D. Reasor, J. Gamache, and F. D. Marks Jr., 2012: Multiscale analysis of tropical cyclone kinematic structure from airborne Doppler radar composites. *Mon. Wea. Rev.*, **140**, 77–99, doi:10.1175/MWR-D-10-05075.1.

——, and Coauthors, 2013a: NOAA's Hurricane Intensity Forecasting Experiment: A progress report. *Bull. Amer. Meteor. Soc.*, **94**, 859–882, doi:10.1175/BAMS-D-12-00089.1.

——, P. Reasor, and S. Lorsolo, 2013b: Airborne Doppler observations of the inner-core structural differences between intensifying and steady-state tropical cyclones. *Mon. Wea. Rev.*, **141**, 2970–2991, doi:10.1175/MWR-D-12-00357.1.

——, P. D. Reasor, and J. A. Zhang, 2015: Multiscale structure and evolution of Hurricane Earl (2010) during rapid intensification. *Mon. Wea. Rev.*, **143**, 536–562, doi:10.1175/MWR-D-14-00175.1.

——, J. A. Zhang, J. Zawislak, H. Jiang, G. R. Alvey III, E. J. Zipser, and S. N. Stevenson, 2016: Observations of the structure and evolution of Hurricane Edouard (2014) during intensity change. Part II: Kinematic structure and the distribution of deep convection. *Mon. Wea. Rev.*, **144**, 3355–3376, doi:10.1175/MWR-D-16-0017.1.

Shay, L. K., and J. K. Brewster, 2010: Oceanic heat content variability in the eastern Pacific Ocean for hurricane intensity forecasting. *Mon. Wea. Rev.*, **138**, 2110–2131, doi:10.1175/2010MWR3189.1.

Stern, D. P., and F. Zhang, 2016: The Warm-Core Structure of Hurricane Earl (2010). *J. Atmos. Sci.*, **73**, 3305–3328, doi:10.1175/JAS-D-15-0328.1.

——, G. H. Bryan, and S. D. Aberson, 2016: Extreme low-level updrafts and wind speeds measured by dropsondes in tropical cyclones. *Mon. Wea. Rev.*, **144**, 2177–2204, doi:10.1175/MWR-D-15-0313.1.

Stevenson, S. N., K. L. Corbosiero, and J. Molinari, 2014: The convective evolution and rapid intensification of Hurricane Earl (2010). *Mon. Wea. Rev.*, **142**, 4364–4380, doi:10.1175/MWR-D-14-00078.1.

Susca-Lopata, G., J. Zawislak, E. J. Zipser, and R. F. Rogers, 2015: The role of observed environmental conditions and precipitation evolution in the rapid intensification of Hurricane Earl (2010). *Mon. Wea. Rev.*, **143**, 2207–2223, doi:10.1175/MWR-D-14-00283.1.

Uhlhorn, E. W., P. G. Black, J. L. Franklin, M. Goodberlet, J. Carswell, and A. S. Goldstein, 2007: Hurricane surface wind measurements from an operational Stepped Frequency Microwave Radiometer. *Mon. Wea. Rev.*, **135**, 3070–3085, doi:10.1175/MWR3454.1.

Velden, C., T. Olander, D. Herndon, and J. Kossin, 2017: Reprocessing the most intense historical tropical cyclones in the satellite era using the advanced Dvorak technique. *Mon. Wea. Rev.*, **145**, 971–983, doi:10.1175/MWR-D-16-0312.1.

Zhang, F., and J. A. Sippel, 2009: Effects of moist convection on hurricane predictability. *J. Atmos. Sci.*, **66**, 1944–1961, doi:10.1175/2009JAS2824.1.